Inhibition of HIV infection by structural proteins of the inner nuclear membrane is associated with reduced chromatin dynamics

Anvita Bhargava, Alice Williart, Mathieu Maurin, Patricia Davidson, Mabel Jouve, Matthieu Piel, Xavier Lahaye, Nicolas Manel

Cell Reports

Article

Inhibition of HIV infection by structural proteins of the inner nuclear membrane is associated with reduced chromatin dynamics

Graphical abstract

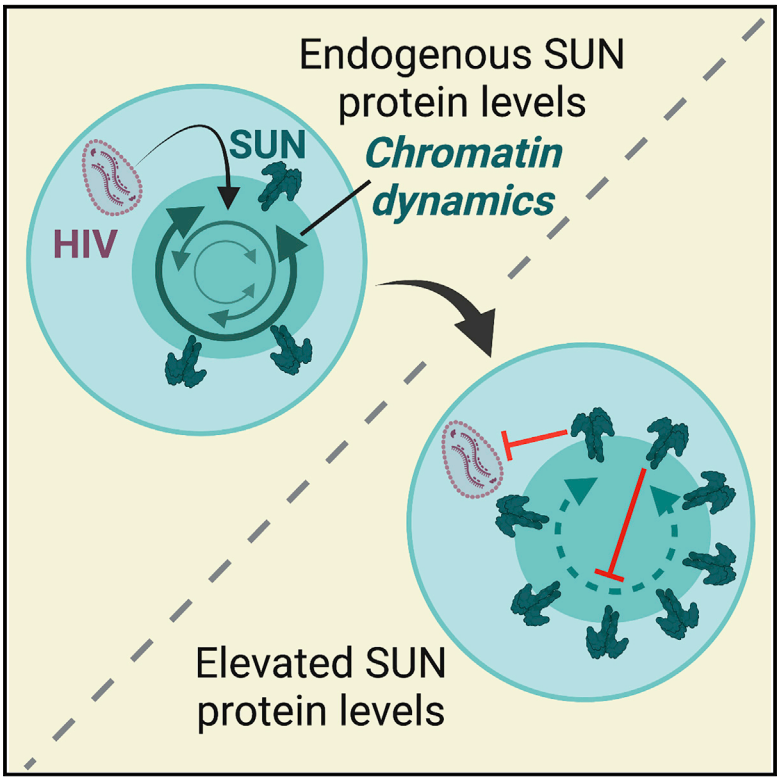

Highlights

- SUN1 and SUN2 show strain-specific antiviral activities against HIV-1 and HIV-2
- The DNA damage response is implicated in the antiviral effect of SUN proteins on HIV-1
- SUN proteins inhibit nuclear rotation and chromatin movements

Authors

Anvita Bhargava, Alice Williart, Mathieu Maurin, ..., Matthieu Piel, Xavier Lahaye, Nicolas Manel

Correspondence

nicolas.manel@curie.fr

In brief

Elevated levels of nuclear envelope proteins SUN1 and SUN2 inhibit HIV infection through an unresolved mechanism. Here, Bhargava et al. show that SUN proteins inhibit nuclear rotation and chromatin movements, indicating a role for chromatin dynamics and the DNA damage response in the control of HIV infection.

Bhargava et al., 2021, Cell Reports *36*, 109763
September 28, 2021
https://doi.org/10.1016/j.celrep.2021.109763

CellPress

Cell Reports

CellPress
OPEN ACCESS

Article

Inhibition of HIV infection by structural proteins of the inner nuclear membrane is associated with reduced chromatin dynamics

Anvita Bhargava,[1] Alice Williart,[2] Mathieu Maurin,[1] Patricia M. Davidson,[3,5] Mabel Jouve,[4] Matthieu Piel,[2] Xavier Lahaye,[1,6] and Nicolas Manel[1,6,7,*]

[1]Institut Curie, PSL Research University, INSERM U932, Paris, France
[2]Institut Curie, PSL Research University, CNRS UMR144, Paris, France
[3]Laboratoire Physico-Chimie Curie, Institut Curie, CNRS UMR168, Sorbonne Université, PSL Research University, Paris, France
[4]Institut Curie, UMR3215, Paris, France
[5]Present address: 4Dcell, Montreuil, France
[6]These authors contributed equally
[7]Lead contact
*Correspondence: nicolas.manel@curie.fr
https://doi.org/10.1016/j.celrep.2021.109763

SUMMARY

The human immunodeficiency virus (HIV) enters the nucleus to establish infection, but the role of nuclear envelope proteins in this process is incompletely understood. Inner nuclear transmembrane proteins SUN1 and SUN2 connect nuclear lamins to the cytoskeleton and participate in the DNA damage response (DDR). Increased levels of SUN1 or SUN2 potently restrict HIV infection through an unresolved mechanism. Here, we find that the antiviral activities of SUN1 and SUN2 are distinct. HIV-1 and HIV-2 are preferentially inhibited by SUN1 and SUN2, respectively. We identify DNA damage inducers that stimulate HIV-1 infection and show that SUN1, but not SUN2, neutralizes this effect. Finally, we show that chromatin movements and nuclear rotations are associated with the effects of SUN proteins and Lamin A/C on infection. These results reveal an emerging role of chromatin dynamics and the DDR in the control of HIV infection by structural components of the nuclear envelope.

INTRODUCTION

Successful infection of cells by the human immunodeficiency virus (HIV) requires an active transport of the virus through the physical barrier of the nuclear envelope. Nuclear entry of HIV is coordinated with the completion of reverse transcription and selection of integration sites (Dharan et al., 2020; Schaller et al., 2011). The capsid (CA) protein of HIV engages multiple interactions with nuclear pore complex (NPC) components and associated proteins such as cyclophilin A (CypA) to achieve this coordination (Yamashita and Engelman, 2017).

In the nuclear envelope, in addition to NPC proteins, SUN proteins located at the inner nuclear membrane impact HIV infection (Bhargava et al., 2018). SUN1 and SUN2 are integral proteins of the inner nuclear envelope of somatic cells. They play essential roles in the maintenance of genomic stability and the resolution of DNA damage (Lawrence et al., 2016; Lei et al., 2012). SUN proteins possess a lamin-binding domain at their N terminus located in the nucleoplasm. Lamins are intermediate filament proteins that assemble the nuclear lamina, a dense meshwork contributing to mechanical protection, organization of chromatin domains, and recruitment of DNA repair factors (Burke and Stewart, 2013; Gonzalo, 2014). At their C terminus, SUN proteins interact with the KASH domains of nesprins in the perinuclear space. Nesprins are large integral proteins of the outer nuclear membrane (Burke and Stewart, 2013). Nesprins have multiple interactions with cytoskeletal proteins, enabling a dynamic anchoring of the nucleus within the cells.

SUN2 was first identified as an antiviral factor against HIV-1 in the context of a cDNA screen (Schoggins et al., 2011). Subsequent studies confirmed and extended the antiviral viral effect of SUN1 and SUN2 overexpression on HIV-1 and HIV-2 infection (Donahue et al., 2016; Lahaye et al., 2016; Luo et al., 2018; Schaller et al., 2017). SUN1 and SUN2 overexpression limits the level of HIV-1 nuclear import (Donahue et al., 2016; Luo et al., 2018; Schaller et al., 2017), leading to reduced viral integration. Furthermore, nanotubes of HIV-1 capsid and nucleocapsid proteins produced *in vitro* pull down SUN1 and SUN2 proteins from cell lysates, suggesting that SUN proteins and the viral capsid protein may interact directly or indirectly during infection (Schaller et al., 2017).

The role of endogenous SUN2 in HIV-1 infection has been examined, but a consensus has not been reached (Donahue et al., 2017; Lahaye et al., 2016; Schaller et al., 2017; Sun et al., 2018). Three studies concurred with a requirement for SUN2 in HIV-1 infection in primary CD4$^+$ T cells, in

monocyte-derived dendritic cells, and in THP-1 cells, although the strength of this requirement varies between cell type (Donahue et al., 2017; Lahaye et al., 2016; Schaller et al., 2017). A fourth study obtained contradicting results and proposed that endogenous SUN2 instead limits HIV infection at the level of viral promoter expression (Sun et al., 2018). We initially proposed that HIV infection requires an optimal level of SUN2 protein, and that both depletion and overexpression impair infection, not necessarily through the same mechanism (Lahaye et al., 2016). This notion fits well with the structural role of the LINC complex in nuclear architecture. Of note, endogenous SUN2 level varies with the extent of T cell activation (Sun et al., 2018). It is thus conceivable that variable experimental conditions between studies, particularly using sensitive primary immune cells, could account for the variable effects of endogenous SUN2 on HIV infection. SUN2 is also implicated in the effects of cyclophilin A on HIV-1 infection. In HeLa cells, SUN2 overexpression abrogates the sensitivity of the HIV-1 capsid mutant N74D to cyclophilin A inhibition (Lahaye et al., 2016). In primary $CD4^+$ T cells and murine bone marrow-derived dendritic cells, endogenous SUN2 is required for the cyclophilin A-dependent steps of HIV infection (Lahaye et al., 2016). Another study, however, did not observe this effect in primary $CD4^+$ T cells (Donahue et al., 2017). These differences may reflect the use of different readouts for quantifying the impact of cyclophilin A inhibition on infection.

Our understanding of the antiviral effect of SUN1 is less advanced. In HEK293A cells, the antiviral effect of SUN1 overexpression requires the interaction of cyclophilin A with HIV-1 capsid protein (Luo et al., 2018). In THP-1 cells, endogenous SUN1 is not required for HIV-1 infection (Schaller et al., 2017).

The strong antiviral effect of SUN protein overexpression on HIV infection exploits one or several points of weakness in the viral replication cycle. The cellular mechanisms by which elevated levels of SUN expression block HIV infection are not known. Intriguingly, SUN2 overexpression is associated with alteration of nuclear envelope shape, suggesting that SUN might interfere with HIV infection through a perturbation of the integrity of the nucleus (Donahue et al., 2016; Lahaye et al., 2016). However, it has not been possible so far to explain how SUN proteins are perturbing cellular and nuclear physiology to impact HIV.

RESULTS

SUN1 and SUN2 proteins demonstrate HIV-strain-specific antiviral effects

To gain insights in SUN1- and SUN2-mediated antiviral effects on the early steps of HIV infection, we first performed a comparative assessment of the antiviral effect of SUN1 and SUN2 on HIV infection in primary cells. To this end, we overexpressed SUN1 and SUN2 in primary monocyte-derived macrophages (MDMs) using lentiviral vectors (Figure 1A). In order to focus on the early phase of infection, cells were infected using single-round HIV-1 and HIV-2 encoding GFP in the place of the Nef gene. SUN1 and SUN2 induced an antiviral effect on HIV-1 and HIV-2 (Figure 1B). Unexpectedly, SUN1 and SUN2 did not show an identical antiviral effect on the two strains. The calculation of the ratio of inhibition by SUN1 over SUN2 revealed that HIV-1 was preferentially inhibited by SUN1, while HIV-2 was preferentially inhibited by SUN2 (Figure 1B). In MDMs, HIV-1 infection is sensitive to inhibition by cyclosporin A (CsA) (Saini and Potash, 2006), and we previously showed that SUN2 overexpression blocks the effect of CsA on infection in other cell types (Lahaye et al., 2016). Here, SUN1 and SUN2 also blocked the effect of CsA on HIV-1 infection in MDMs (Figure 1B). Although not the primary focus of this study, this strengthens the notion that the SUN1 and SUN2 antiviral effects implicate a CsA-sensitive step of HIV infection. We next analyzed the progression of HIV-1 and HIV-2 infection in the context of SUN protein expression using quantitative real-time PCR on viral DNA species, using reverse transcriptase inhibitors as controls (Figure S1A). SUN1 and SUN2 overexpression had no significant impact on the total amount of HIV-1 DNA, but they reduced the levels of 2-long terminal repeat (LTR) circles, which are a hallmark of viral entry into the nucleus, and of integrated viral DNA (Figure 1C). The reduction of HIV-1 integrated DNA was more significant for SUN1 than SUN2, while it was the opposite for HIV-2. These experiments indicate that SUN1 and SUN2 impact the nuclear steps of HIV infection but have strain-specific antiviral effects.

We similarly overexpressed SUN1 and SUN2 in HeLa cells (Figure 2A). SUN1 overexpression had a greater inhibitory effect on HIV-1 infection than on SUN2 overexpression, whereas in HIV-2 infection, SUN2 overexpression had a greater effect than SUN1, recapitulating the results obtained in MDMs (Figures 2B and 2C). In HeLa cells, wild-type (WT) HIV-1 is not sensitive to CsA, but HIV-1 capsid N74D is, similar to HIV-1 WT in MDMs (De Iaco and Luban, 2014). We thus used this mutant to address the relationship between the antiviral effect of SUN and CsA sensitivity. Both SUN1 and SUN2 abolished CsA sensitivity of HIV-1 capsid N74D in HeLa cells (Figures 2D and 2E). We next measured the levels of HIV-1 DNA species. SUN1 and SUN2 reduced the levels of integrated HIV-1 DNA, and this effect was more pronounced for SUN1 (Figure S1B). We also observed a small but significant inhibition of total viral DNA levels by SUN1 and of 2-LTR circles by SUN2. We compared the antiviral effects of SUN1 and SUN2 on different HIV-1 strains. The antiviral effect of SUN1 was more important than that of SUN2 for all HIV-1 lab strains (NL4-3, Lai, JR-CSF, and YU-2) and transmitter/founder strains (THRO, CH058, and CH077) tested. In contrast, the antiviral effect of SUN2 was more important than that of SUN1 for two HIV-2 strains tested (ROD9 and JK71312As) (Figure 2F). Of note, HIV-1 Lai and JR-CSF were resistant to SUN2, while JK7312As was resistant to SUN1. We thus focused on HeLa cells for additional experiments aimed at characterizing the strain-specific inhibition of SUN1 and SUN2.

Strain-specific antiviral activity maps to the nucleoplasmic domain of SUN proteins

Cell-cell communication factors of innate immunity, such as interferons and cyclic guanosine monophosphate-adenosine monophosphate (cGAMP), can contribute to antiviral effects on top of cell-intrinsic restriction factors. Using a co-culture of SUN1/2-expressing cells and control cells expressing a fluorescent marker (TagRFP657), we found that the strain-specific effect of SUN1 and SUN2 on HIV-1 and HIV-2 infection is entirely cell-intrinsic in HeLa cells (Figure 3A). To determine whether SUN1 and SUN2 induced an antiviral state at the cell-intrinsic

CellPress
OPEN ACCESS

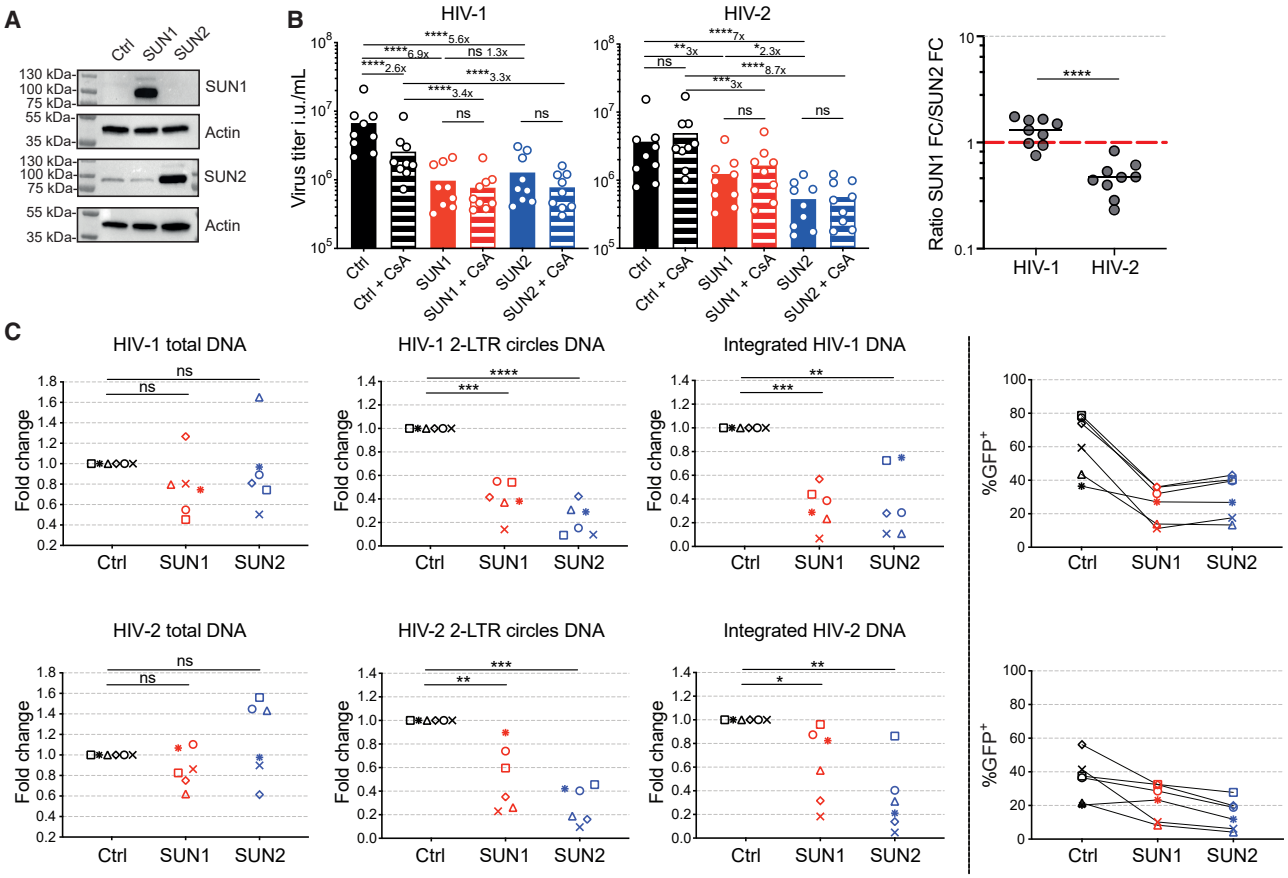

Figure 1. Distinct antiviral activities of SUN1 and SUN2 against HIV-1 and HIV-2 in primary macrophages

(A) Detection of SUN1, SUN2, and actin in MDMs transduced with mTagBFP-2A control, SUN1, or SUN2 lentivectors (representative of n = 3).

(B) (Left) Viral titers as infectious units (IU) per mL based on percentages of GFP$^+$ MDMs 48 h after infection with serial dilutions of HIV-1 or HIV-2 encoding GFP in Nef and pseudotyped with vesicular stomatitis virus glycoprotein G (VSV-G), with or without 2 μM CsA (n = 9 donors, paired repeated measures (RM) one-way ANOVA on log-transformed titers with a Sidak's post-test, line at mean). (Right) Ratios of titer fold change (FC) control over SUN1 (SUN1 FC) or control over SUN2 (SUN2 FC) (paired t test, line at mean).

(C) (Left) Detection of HIV-1 total DNA, 2-LTR circles DNA, and integrated DNA by quantitative real-time PCR at 24 h after infection with HIV-1 or HIV-2 (dilution factor, 0.17) of MDMs transduced with mTagBFP (blue fluorescent protein)-2A control, SUN1, or SUN2 lentivectors. (Right) Infection levels for each donor (n = 6 donors, quantitative real-time PCR data are represented as donor-matched fold change compared to control; one-sample t test).

Ctrl, control. *p < 0.05, **p < 0.01, ***p < 0.001, ****p < 0.0001; ns, not significant. See also Figure S1.

level through expression of other antiviral genes, we performed a transcriptomic analysis of SUN1 and SUN2 overexpressing cells. Strikingly, we could not detect any differentially expressed genes in this dataset, aside from SUN1 and SUN2 themselves (Figure S1C). Next, we generated chimeras between SUN1 and SUN2 to map the strain-specific antiviral effect (Figures 3B and 3C). We found that the N-terminal nucleoplasmic domains of SUN1 and SUN2 confer strain specificity (Figures 3D and 3E). These results establish that SUN1 and SUN2 exert a cell-intrinsic HIV-strain-specific antiviral effect on HIV infection that maps to the nucleoplasmic domain of SUN proteins.

Interplay between SUN proteins, HIV infection, and the DNA damage response

As a next step, we attempted to characterize the cellular processes affected by elevated levels of SUN proteins. SUN1 and SUN2 are required to limit the accumulation of DNA damage in cells (Lei et al., 2012). Since HIV infection is a DNA-damaging event, we considered the possible interplay between SUN proteins, HIV infection, and the DNA damage response. We examined the level of γH2AX, an early marker of the DNA damage response. At baseline, we did not detect any change of γH2AX levels upon SUN1 or SUN2 expression (Figures 4A and 4B). To induce DNA damage, we selected etoposide, a topo-isomerase II inhibitor. Interestingly, SUN1 overexpression but not SUN2 significantly limited the levels of induced γH2AX after etoposide treatment (Figures 4A and 4B). To explore the potential link between DNA damage and infection, we infected HeLa cells in the presence of etoposide for the first 4 h of the experiment. However, etoposide gradually induces apoptosis of treated cells (Rello-Varona et al., 2006), which hampered our ability to detect viable cells to measure infection after 48 h. To circumvent this,

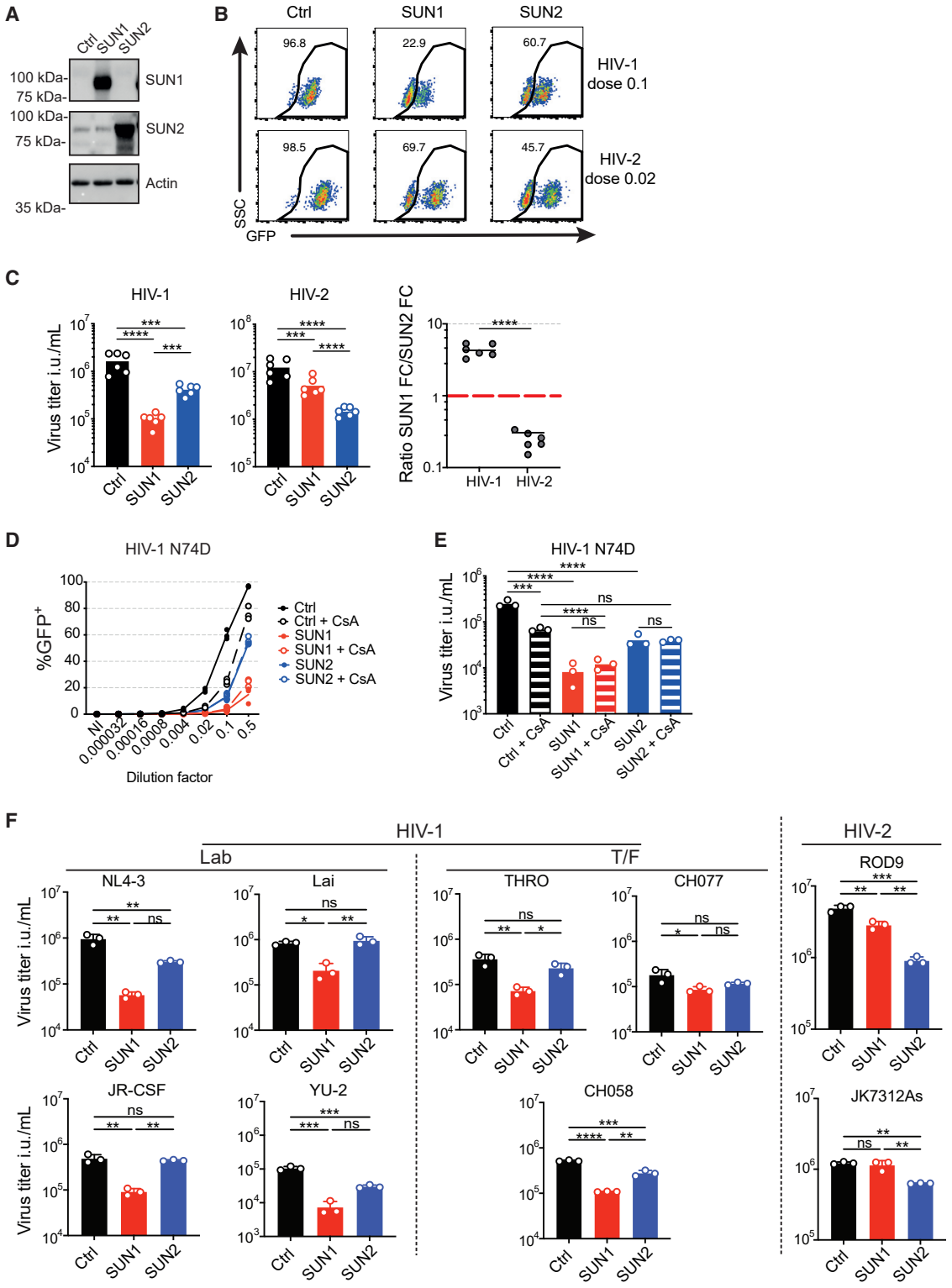

Figure 2. Distinct antiviral activities of SUN1 and SUN2 against multiple HIV-1 and HIV-2 strains in HeLa cells

(A) Detection of SUN1, SUN2, and actin in HeLa cells transduced with mTagBFP-2A control, SUN1, or SUN2 lentivectors.

(B) GFP expression in BFP$^+$ HeLa cells transduced with mTagBFP-2A control, SUN1, or SUN2 lentivectors, 48 h after infection with indicated dilutions of HIV-1 and HIV-2 (representative data from one experiment at the indicated dose of virus).

(legend continued on next page)

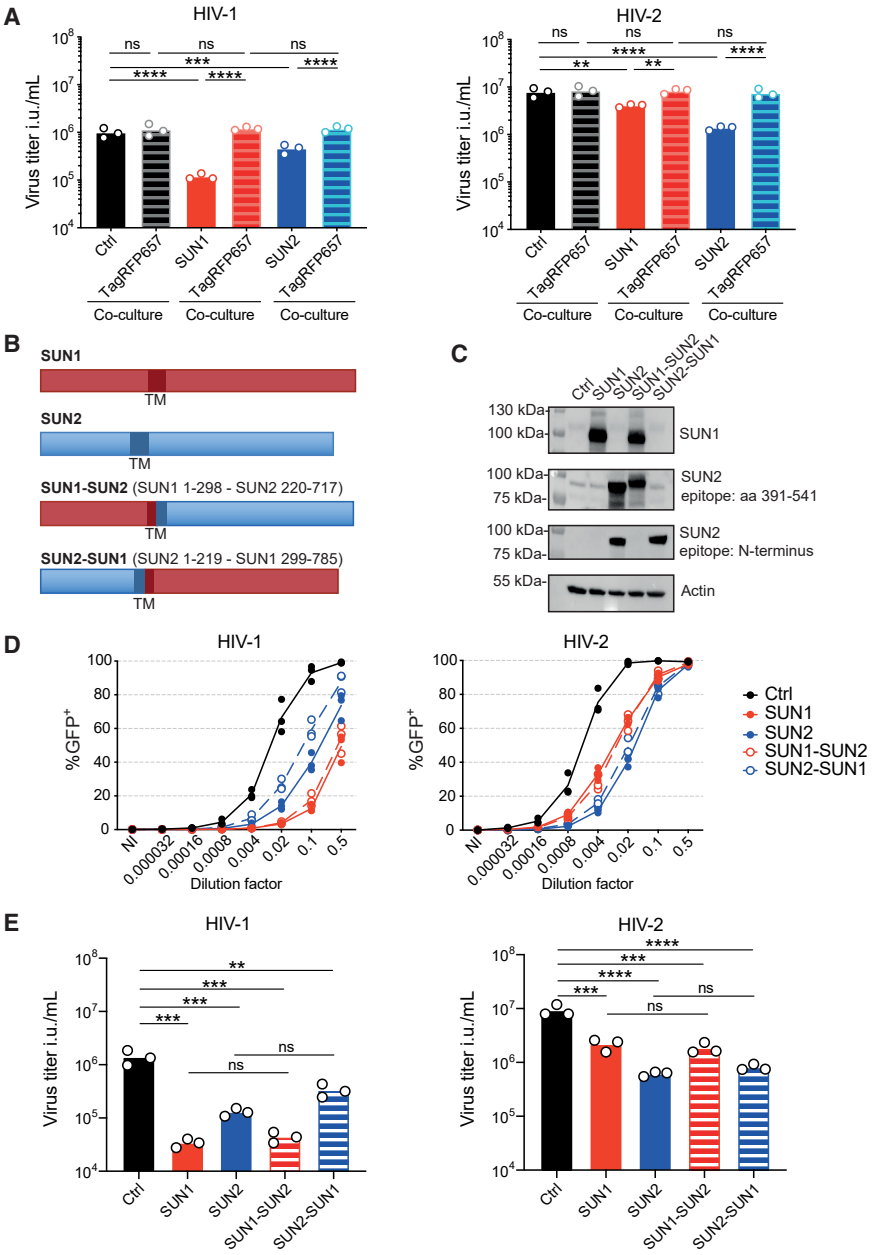

Figure 3. Mapping of the strain-specific antiviral activity of SUN proteins

(A) mTagBFP-2A Ctrl, mTagBFP-2A-SUN1, and mTagBFP-2A-SUN2 expressing HeLa cells were co-cultured at a 1:1 ratio with HeLa cells expressing TagRFP657-2A and infected with serial dilutions of HIV-1 and HIV-2. Titers were calculated based on the percentage of GFP$^+$ cells in 48-h post-infection dilutions within the indicated populations (n = 3 independent experiments, paired RM one-way ANOVA on log-transformed titers with Sidak's post-test, line at mean).

(B) Schematic representation of chimeric proteins between full-length SUN1 (red) and SUN2 (blue). Amino acid residues retained in hybrid proteins are indicated within brackets.

(C) Detection of SUN1, SUN2, and actin in HeLa cells transduced with the indicated mTagBFP-2A lentivectors. Two antibodies targeting SUN2 that recognize different epitopes within the protein were used.

(D) Percentage of GFP$^+$ in BFP$^+$ HeLa cells transduced with the indicated mTagBFP-2A lentivectors, 48 h after infection with serial dilutions of HIV-1 or HIV-2 (n = 3 independent experiments).

(E) Viral titers based on percentages of GFP$^+$ cells shown in (D) (n = 3, paired RM one-way ANOVA with Sidak's post-test, line at mean).

**p < 0.01, ***p < 0.001, ****p < 0.0001; ns, not significant. See also Figure S1.

we cultured cells in the presence of the caspase inhibitor Q-VD-Oph and lower doses of etoposide. Q-VD-Oph did not prevent γH2AX induction by etoposide treatment (Figure 4C). Etoposide treatment increased HIV-1 infection by 2-fold on average (Figure 4D). HIV-2 infection was also increased but significantly at only one dose of etoposide tested, with a smaller fold change. Next, we combined SUN expression with etoposide to determine the epistatic relationship between DNA damage induction and SUN expression on the level of HIV infection. Here, we used a higher MOI to observe the antiviral effect of SUN proteins. The increase induced by etoposide treatment on control cells was consistently observed across experiments. Interestingly, SUN1 abrogated the proviral effect of etoposide treatment and, in sharp contrast, etoposide treatment rescued cells from the antiviral effect of SUN2 (Figures 4E and 4F). We next explored the effects of bleomycin, which induces direct double-stranded DNA breaks akin to etoposide. Bleomycin induced upregulation of γH2AX (Figure S2A). SUN1 slightly reduced this

(C) (Left) Viral titers based on percentages of GFP$^+$ cells after infection with serial dilutions of the indicated viruses (n = 6, paired RM one-way ANOVA on log-transformed titers, with Tukey's post-test, line at mean). (Right) ratios of titer FC control over SUN1 (SUN1 FC) or control over SUN2 (SUN2 FC) (paired t test, line at mean).

(D) Percentage of GFP$^+$ in BFP$^+$ HeLa cells transduced with mTagBFP-2A control, SUN1, or SUN2 lentivectors, 48 h after infection with serial dilutions of HIV-1 or HIV-1 capsid N74D, with or without treatment with 2 μM of CsA (n = 3 independent experiments).

(E) Viral titers as in (D) (n = 3, paired RM one-way ANOVA on log-transformed titers with Sidak's post-test, line at mean).

(F) Viral titers based on percentages of GFP$^+$ or p24$^+$ cells after infection with serial dilutions of indicated HIV-1 and HIV-2 viral strains (n = 3, paired RM one-way ANOVA with Sidak's post-test, line at mean + SD).

*p < 0.05, **p < 0.01, ***p < 0.001, ****p < 0.0001; ns, not significant. See also Figure S1.

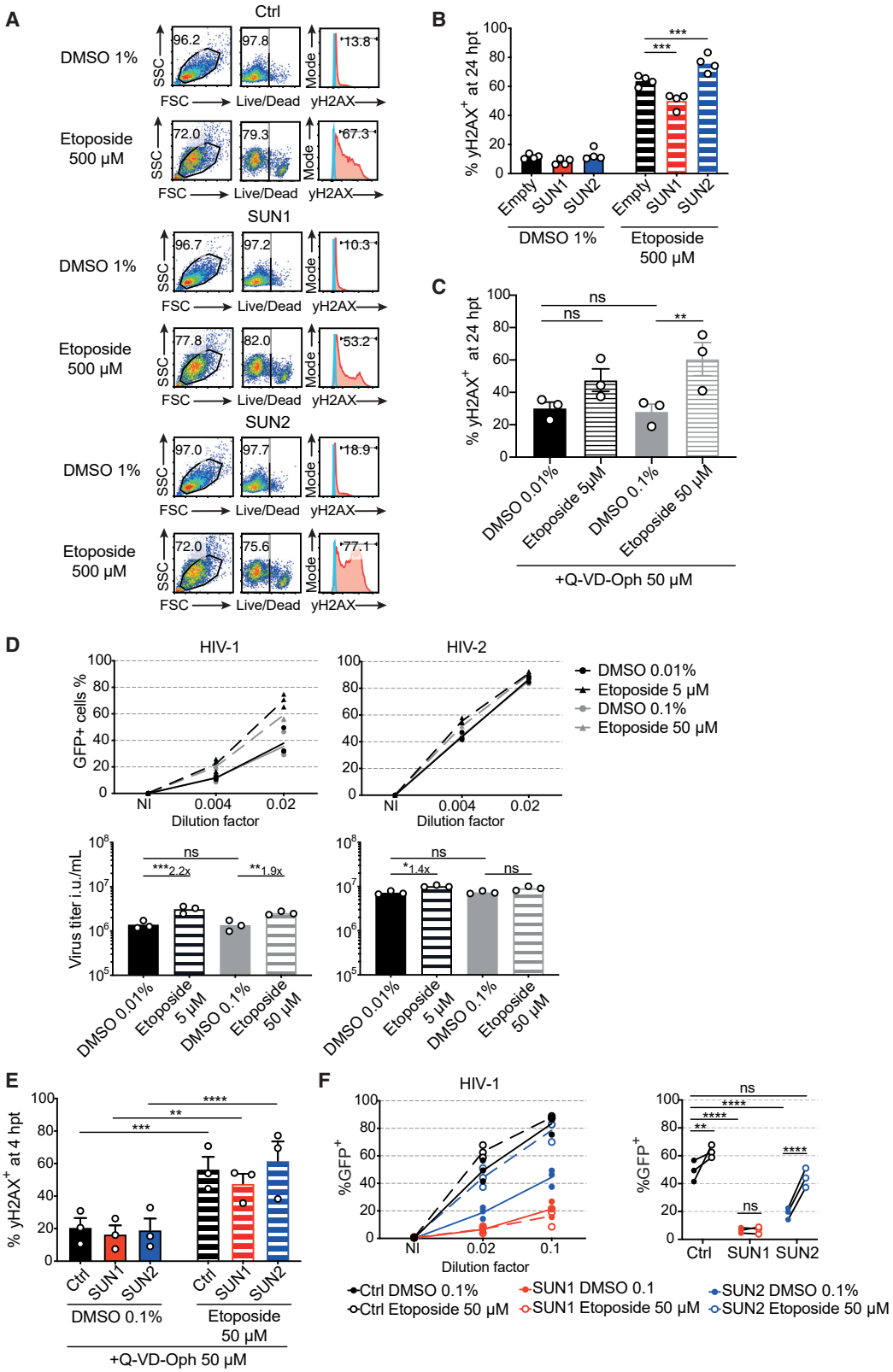

(legend on next page)

induction in all experiments, while SUN2 had no impact. Similar to etoposide, HIV-1 infection was increased by bleomycin treatment (Figure S2B). This pro-viral effect of bleomycin was lost upon SUN1 expression, while it was consistently maintained with SUN2. Next, we tested hydroxyurea and UV treatments, which cause DNA damage rather through DNA replication stress. Both treatments induced upregulation of γH2AX (Figure S2C). However, they did not have an effect on the rate of HIV-1 infection (Figure S2D), indicating that HIV infection is modulated by only a subset of DNA damaging agents. Overall, these results show that SUN1 overexpression, which restricts HIV-1 infection more than SUN2, operates downstream of DNA damage induction, while SUN2 overexpression impacts infection upstream of DNA damage induction.

DNA damage induction by ATR inhibition and role of HIV-1 Vpr

Next, we looked for a different approach to induce DNA damage that would be functionally linked to the nuclear envelope. ATR is a DNA damage sensor that functions as a checkpoint at the nuclear envelope in response to mechanical stress (Kumar et al., 2014). ATR inhibition heightens DNA damage in cells (Foote et al., 2018). Furthermore, in HIV-1, expression of the accessory protein Vpr causes DNA damage and activates ATR (Roshal et al., 2003), although the relevance of this effect in the context of virion-packaged Vpr is unknown. Considering the significance of ATR at the nuclear envelope and its relationship with Vpr, we asked whether DNA damage induction by ATR inhibition, SUN, and Vpr are functionally related. We inhibited ATR using AZD6738, a next-generation inhibitor with improved specificity (Foote et al., 2018). As expected, ATR inhibition increased the levels of γH2AX in HeLa cells (Figure S3A). We next infected HeLa cells with p24-normalized and sucrose cushion purified stocks of the HIV-1 single-round virus and its HIV-1 Vpr-deficient (Vpr^-) counterpart. ATR inhibition increased Vpr-positive HIV-1 infection in HeLa cells by 2-fold, similar to etoposide treatment (Figure S3B, left panel). Concomitant SUN protein overexpression inhibited HIV-1 infection and reduced the magnitude of the proviral effect of ATR inhibition. Unexpectedly, the titer of the p24-normalized HIV-1 Vpr^- was slightly higher than the HIV-1 WT counterpart in HeLa cells, and HIV-1 Vpr^- was insensitive to ATR inhibition (Figure S3B, right panel). However, HIV-1 Vpr^- remained sensitive to the antiviral effect of SUN protein expression. In sum, these data implicate the kinase ATR in limiting HIV infection of HeLa cells. Intriguingly, the data also revealed that sensitivity to ATR inhibition is a HIV-1 Vpr phenotype in single-round infection of HeLa cells.

Endogenous Lamin A/C limits HIV-1 infection in HeLa cells

We sought to further explore the relationship between infection, DNA damage, and structure of the nuclear envelope. Electron microscopy analysis revealed that both SUN1 and SUN2 overexpression induced deep invaginations of the nuclear envelope, which appeared more pronounced with SUN2 (Figure 5A). This raised the possibility that alteration of the shape of the nucleus could be responsible for the antiviral effect. We searched for an orthogonal approach to perturb the nuclear envelope structure and the DNA damage response. Lamin A/C expression is required to maintain a regular nuclear shape (Lammerding et al., 2004) and to protect from DNA damage (Singh et al., 2013). We used short hairpin RNA (shRNA) to reduce expression of Lamin A/C (Figure 5B). Similar to SUN protein overexpression, knockdown of Lamin A/C compromised the regularity of the nuclear envelope shape (Figure 5C). To quantify this effect, we measured the shape descriptor "solidity" of the nucleus: solidity values close to 1 indicate smoothly convex nuclei while lower values correspond to deformed, lobulated nuclei, presenting concave invaginations. Overexpression of SUN proteins and silencing of Lamin A/C increased nuclear envelope deformation, and this effect was less pronounced in cells overexpressing SUN1 compared to SUN2 (Figure 5D). The endogenous levels of Lamin A/C and SUN proteins were not reciprocally affected by SUN overexpression or Lamin A/C silencing. (Figure 5B). After infection, Lamin A/C knockdown unexpectedly increased HIV-1 infection levels by 1.6-fold, while HIV-2 infection was not affected (Figure 5E). Lamin A/C thus limits HIV-1 infection in HeLa cells. Given the opposing effects of SUN overexpression and Lamin A/C knockdown on HIV-1 infection, we examined whether the antiviral effect of SUN proteins requires endogenous lamins. We knocked down Lamin A/C, Lamin B1, and Lamin B2 and co-expressed SUN proteins (Figure 5F). Viable Lamin B1-depleted HeLa cells could not be maintained in culture. Lamin A/C depletion enhanced HIV-1 infection as above, and Lamin B2 depletion had no effect (Figure 5G). SUN proteins maintained their antiviral effect

Figure 4. Interplay between HIV-1 infection, SUN proteins, and the DNA damage response

(A) Viability and γH2AX intracellular staining in HeLa cells transduced with mTagBFP-2A control, SUN1, or SUN2 lentivector, 24 h after treatment with 500 μM etoposide or 1% DMSO as control (representative experiment from n = 3).

(B) Quantification of $γH2AX^+$ HeLa cells treated as in (A) (n = 4, paired RM one-way ANOVA with Sidak's post-test, line at mean).

(C) Quantification of $γH2AX^+$ HeLa cells 24 h after a 4-h treatment with 5 or 50 μM etoposide or corresponding DMSO control. 50 μM Q-VD-Oph was present throughout the experiment (n = 3, paired RM one-way ANOVA with Sidak's post-test, line at mean ± SEM).

(D) (Top) Percentage of GFP^+ HeLa cells 48 h after infection with two dilutions of HIV-1 (plasmid HIVGFP env^-nef^-) or HIV-2. Cells were treated and infected simultaneously, and the drugs and the virus were washed out at 4 h post-treatment/infection. 50 μM Q-VD-Oph was maintained throughout the experiment. (Bottom) Viral titers based on percentages of GFP^+ cells (n = 3, paired RM one-way ANOVA with Sidak's post-test, line at mean).

(E) Quantification of $γH2AX^+$ HeLa cells transduced with mTagBFP-2A control, SUN1, or SUN2 lentivectors, 4 h after treatment with 50 μM etoposide or corresponding DMSO control (n = 3, paired RM one-way ANOVA with Sidak's post-test, line at mean ± SEM).

(F) (Left) Percentage of GFP^+ cells in BFP^+ HeLa cells expressing control, SUN1, or SUN2 lentivectors and treated as in (E), 48 h after infection with purified HIV-1 (plasmid HIVGFP env^-nef^-). Right, GFP^+ percentages at viral dilution 0.02 (n = 3, experimental pairs are indicated; RM ANOVA two-way test, uncorrected Fisher's least significant difference [LSD] test). 50 μM Q-VD-Oph was maintained throughout the experiment.

hpt, hours post-treatment. *p < 0.05, **p < 0.01, ***p < 0.001, ****p < 0.0001; ns, not significant. See also Figures S2 and S3.

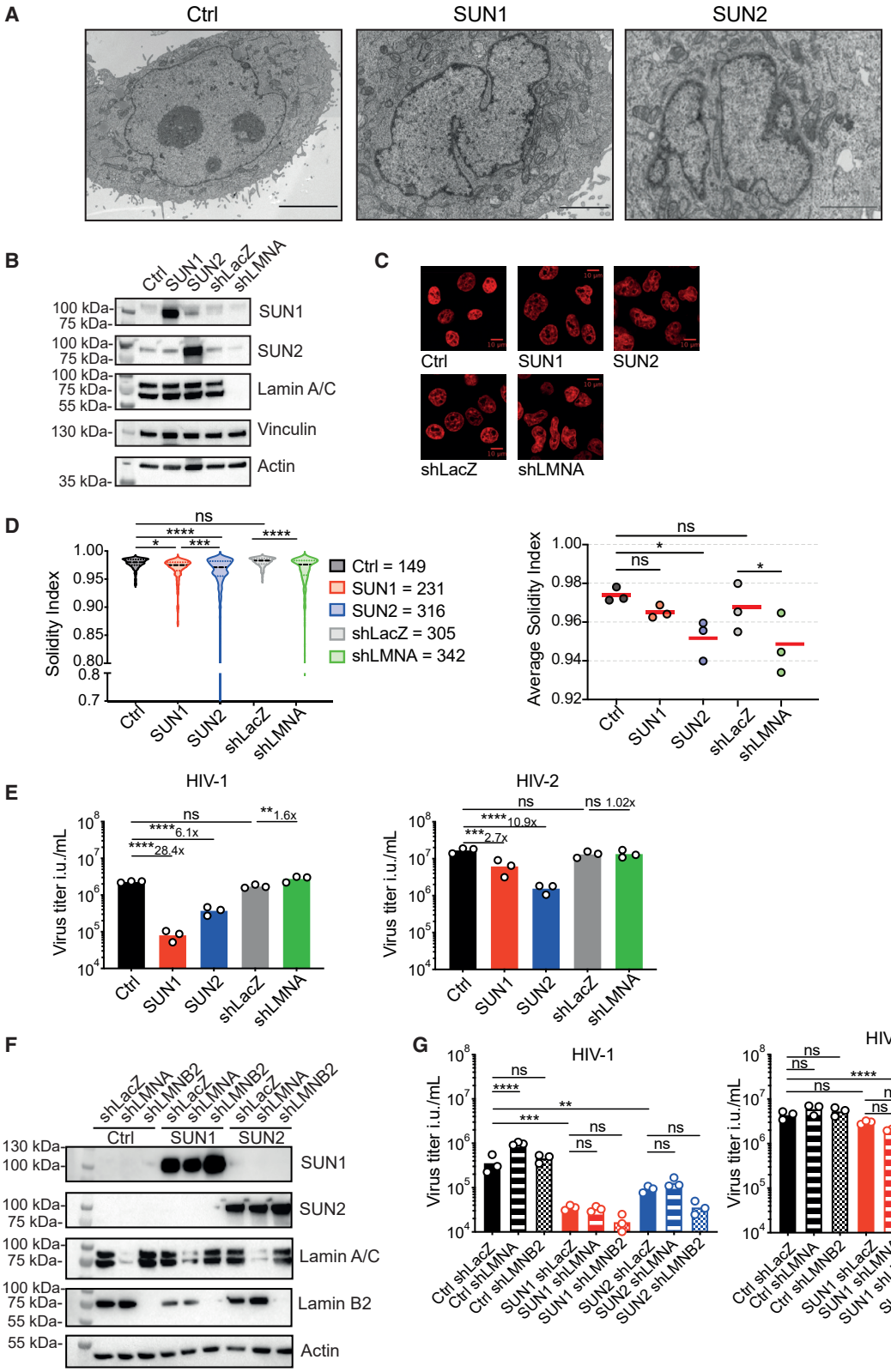

(legend on next page)

irrespective of the level of Lamin A/C and Lamin B2. This shows that the effect of elevated levels of SUN proteins is dominant on the effect of Lamin A/C depletion on HIV-1 infection. Furthermore, these results indicate that the increase in nuclear envelope shape irregularities does not explain how Lamin A/C depletion and SUN protein overexpression affect HIV infection.

Next, we examined the level of γH2AX after etoposide treatment and Lamin A/C depletion. Treatment with a high dose of etoposide (500 μM) for 24 h induced an increase of γH2AX level in WT HeLa cells, while a lower dose (50 μM) had no impact at this time point (Figure S4). In the absence of Lamin A/C, HeLa cells became hypersensitive to etoposide treatment (Figure S4). Thus, the increase in HIV-1 infection observed after Lamin A/C depletion correlates with an increased sensitivity to DNA damage. Altogether, these results establish a functional correlation between the effect of SUN protein and endogenous Lamin A/C on HIV-1 infection and the cellular response to DNA damage induced by an exogenous compound.

Elevated SUN proteins do not alter NPC density, passive import, or cell stiffness

We next sought to identify the mechanisms that delineate the effects of elevated SUN proteins and endogenous Lamin A/C depletion on infection. We characterized biophysical and structural parameters in SUN-expressing cells. HIV-1 enters the nucleus through NPCs. We labeled NPCs using a marker of Nup153 on tangential confocal microscopy sections of the nuclear envelope (Figure S5A). Overexpression of SUN proteins did not alter NPC density at the nuclear envelope (Figure S5B). To determine whether the NPC functionality was impaired by SUN protein overexpression, we measured passive diffusion through the NPC using a fluorescence recovery after photobleaching (FRAP) assay on ubiquitous GFP. SUN proteins had no impact on the rate of recovery of nuclear GFP (Figure S5C; Video S1). Lamin A/C depletion reduces stiffness of the nuclear envelope, resulting in a more deformable nucleus (Lammerding et al., 2004). To determine whether the expression of SUN proteins induced the opposite to match the effects on infection, we measured the viscoelastic properties of the nuclei using a microfluidic micropipette assay (Davidson et al., 2019). While we confirmed that Lamin A/C-depleted cells are more deformable, expression of SUN proteins had no impact on nuclear deformability (Figure S5D).

HIV-1 infection requires movement of the chromatin

Next, we turned our attention to the endogenous state of chromatin. We performed live imaging of cells with a DNA stain after SUN overexpression or Lamin A/C depletion. We observed that SUN1 and SUN2 overexpression appeared to lock the nucleus in place, while nuclei of Lamin A/C-depleted cells appeared highly dynamic (Figure 6A; Video S2). We first asked whether the extent of chromatin movement inside the nuclei was altered. We isolated videos of single nuclei and performed a registration step to normalize x-y positions and angle, therefore suppressing general nuclei displacement and rotation. We next measured chromatin movement in the registered nuclei by performing a particle image velocimetry (PIV) analysis. Strikingly, SUN1 and SUN2 overexpression reduced the displacement of chromatin over time and this effect was more pronounced with SUN1, while Lamin A/C depletion had the converse effect (Figures 6B and 6C). HeLa cells also exhibit seemingly random rotation of their nuclei at various speeds and frequencies. Using the same dataset, we measured the rotation of the whole nucleus relative to the cytoplasm. We corrected the translational displacement of nuclei by registration and measured the angle of rotation over time using a custom-made analysis script (Video S3). SUN1 and SUN2 reduced the average speed of nuclear rotation (Figures 6D and 6E) and the fraction of time spent rotating above a threshold of 1° (Figures S6A and S6B). The rotation of Lamin A/C-depleted nuclei was visibly higher than that of controls but could not be reliably quantified due to the high levels of chromatin displacement that hampered the ability to set reference points.

If SUN proteins inhibit HIV infection by limiting chromatin movements, increasing rotation would be expected to overcome the viral restriction. SUN proteins form the LINC complex with nesprins at the nuclear envelope by interaction with their KASH domain within the perinuclear space. Expression of the isolated KASH domain (spectrin repeat-KASH, SR-KASH) functions as a dominant negative by disrupting the SUN-nesprin interaction and displacing nesprins from the nuclear envelope (Starr et al., 2003). We co-expressed SR-KASH with SUN proteins (Figure 7A; Video S4). Strikingly, SR-KASH increased the rotation speed of chromatin in control and SUN-overexpressing cells (Figures 7B

Figure 5. SUN proteins inhibit HIV infection at the nuclear envelope independently of endogenous lamins

(A) Representative electron micrograph showing nuclei in control, SUN1, and SUN2 overexpressing HeLa cells (scale bars, 10, 2, and 5 μm, respectively).

(B) Detection of SUN1, SUN2, Lamin A/C, and actin in HeLa cells transduced with mTagBFP-2A control, SUN1, or SUN2 lentivectors, negative control LacZ (shLacZ), or Lamin A/C (shLMNA) targeting shRNA-encoding lentivectors.

(C) Nuclei of HeLa cells lines as in (B) visualized on fixed cells using SiR-DNA dye. Images show signal from an individual, central confocal plane. Scale bars, 10 μm.

(D) Solidity index of nuclei as in (C). (Left) Data from one representative experiment out of three. Legend indicates total number of nuclei analyzed per cell line. Unpaired one-way ANOVA with Sidak's post-test, line at median. (Right) Average solidity index across three independent experiments (paired one-way ANOVA with Sidak's post-test, line at mean).

(E) Viral titers based on percentages of GFP^+ HeLa cells lines from (B) after infection with serial dilutions of HIV-1 and HIV-2 (n = 3, paired RM one-way ANOVA with Sidak's post-test, line at mean).

(F) Detection of SUN1, SUN2, Lamin A/C, Lamin B2, and actin in HeLa cells co-transduced with mTagBFP-2A control, SUN1, or SUN2 lentivectors and with LacZ, Lamin A/C, or Lamin B2 (shLMNB2) targeting shRNA-encoding lentivectors.

(G) Viral titers based on percentages of GFP^+ HeLa cells as shown in (F) after infection with serial dilutions of HIV-1 and HIV-2 (n = 3, paired RM one-way ANOVA with Sidak's post-test, line at mean).

*p < 0.05, **p < 0.01, ***p < 0.001, ****p < 0.0001; ns, not significant. See also Figures S4 and S5 and Video 1.

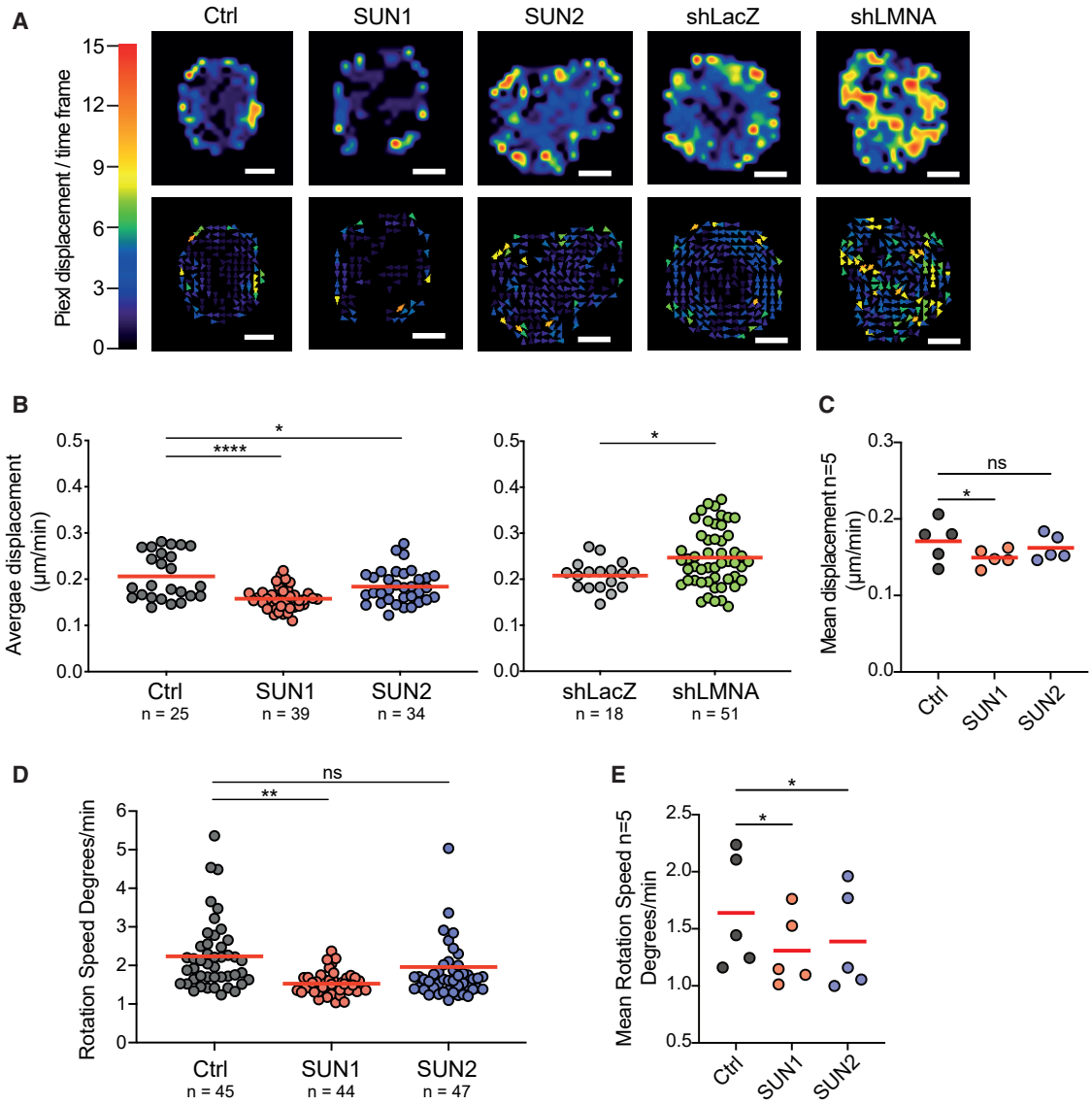

Figure 6. SUN protein overexpression and endogenous Lamin A/C limit movements of the chromatin

(A) Particle image velocimetry (PIV) of DNA within nuclei of HeLa cells transduced with mTagBFP-2A control, SUN1, or SUN2 lentivectors, negative control LacZ, or Lamin A/C targeting shRNA-encoding lentivectors. PIV is shown for individual representative nuclei of each cell line; top panels show overall flow, and bottom panels show individual vectorial displacements between two consecutive frames corresponding to 2 min of imaging. Scale bars, 5 μm. Reference color scale for pixel displacement per time frame is shown on left.

(B) Quantification of DNA displacement as μm/min from images as in (A). Results are shown for one experiment from n = 2. (Left) Unpaired one-way ANOVA with Sidak's post-test, line at mean. (Right) Unpaired Student's t test, line at mean.

(C) Average chromatin displacement within nuclei of HeLa cells transduced with mTagBFP-2A control, SUN1, or SUN2 lentivectors (n = 5 independent experiments, paired one-way ANOVA with Dunnett's post-test, line at mean).

(D) Quantification of nuclear rotation speed as degrees/min in HeLa cells transduced with mTagBFP-2A control, SUN1, or SUN2 lentivectors and imaged as in (A). Results are shown for one experiment from n = 5. Unpaired one-way ANOVA with Sidak's post-test, line at mean.

(E) Average nuclear rotation speed within nuclei of HeLa cells as in (D) (n = 5 independent experiments, paired one-way ANOVA with Holm-Sidak's post-test, line at mean).

*p < 0.05, **p < 0.01, ****p < 0.0001; ns, not significant. See also Figure S6 and Videos S2 and S3.

and 7C) and significantly increased the fraction of time that SUN1-overexpressing cells spent rotating (Figures S6C and S6D). In contrast, SR-KASH had no significant effect on the shape of the nuclei (Figure S6E). Upon HIV-1 infection, SR-KASH partially reverts the antiviral effects of SUN1 and SUN2 (Figure 7D). Overall, these results indicate that the impact of SUN and Lamin A/C proteins on HIV-1 infection is associated with the movement of chromatin within the cells.

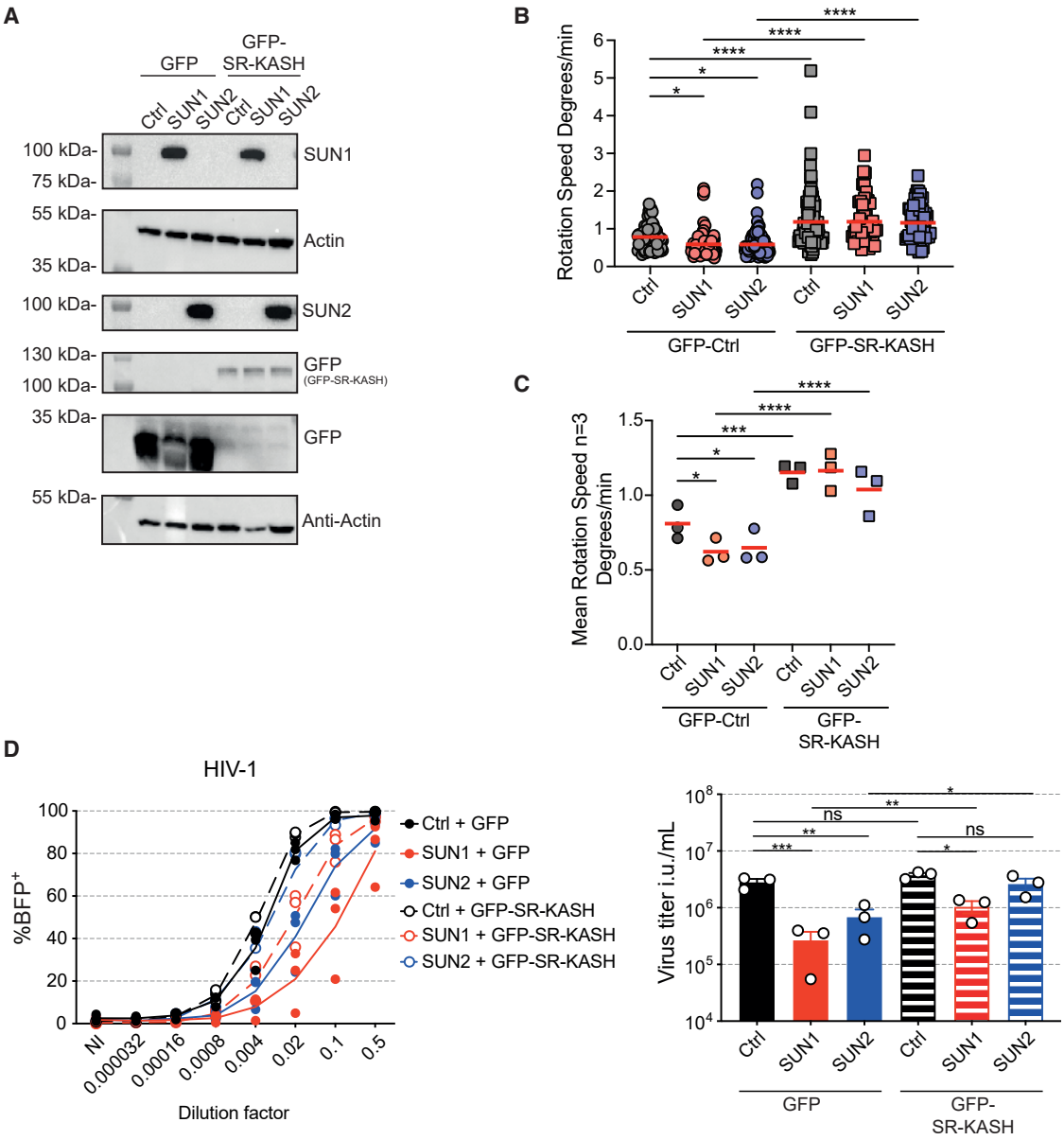

Figure 7. Increased rotations of chromatin limit the SUN-mediated antiviral state

(A) Detection of SUN1, SUN2, GFP, and actin in HeLa cells transduced with TagRFP657-expressing control, SUN1, or SUN2 lentivectors, combined with control GFP or SR-KASH DN fused to GFP-expressing lentivectors. The same lysates were loaded onto two separate membranes; the housekeeping control is shown for both.

(B) Quantification of nuclear rotation speed as degrees/min in HeLa cell lines as in (A), based on images taken every 6 min. Results are shown for one experiment from n = 3. Unpaired one-way ANOVA with Sidak's post-test, line at mean.

(C) Average rotation speed of nuclei as in (B) (n = 3 independent experiments, paired one-way ANOVA with Sidak's post-test, line at mean).

(D) (Left) Percentage of BFP^+ within $tagRFP657^+$ HeLa cells 48 h after infection with serial dilutions of HIV-1 encoding BFP in the place of Nef, pseudotyped with VSV-G. (Right) Viral titers based on percentages of BFP^+ cells (n = 3, paired RM one-way ANOVA on log-transformed titers, with Sidak's post-test, line at mean ± SEM).

*p < 0.05, **p < 0.01, ***p < 0.001, ****p < 0.0001; ns, not significant. See also Figure S6 and Video S4.

DISCUSSION

Our findings reveal that SUN1 and SUN2, although paralogs, have distinct effects on HIV infection. SUN1 overexpression is more efficient at inhibiting HIV-1 than is SUN2. Meanwhile, SUN2 overexpression shows a marked antiviral activity against HIV-2. An analysis of the viral step impacted by these two proteins also reveals differences: SUN1 inhibits more significantly

HIV-1-integrated DNA than does SUN2, while it is the converse for HIV-2. The strain-specific antiviral effects of SUN1 and SUN2 were conserved across all viral clones tested. We also reveal that SUN1 and SUN2 differ in their response to DNA damage and its impact on HIV infection. SUN1 limits the response to etoposide as measured by the levels of γH2AX, while SUN2 enhances the response. Strikingly, etoposide largely rescues the antiviral effect of SUN2 overexpression on HIV-1, while SUN1 is resistant to this effect. This result suggests that SUN1 and SUN2 may differ in the ways in which they establish interactions and functions within the nucleus, in line with previously reports showing non-redundant effects of SUN1 and SUN2 (Lei et al., 2009; Liu et al., 2007; Zhu et al., 2017)

Etoposide treatment also enhances the infection by HIV-1 by 2-fold in HeLa cells in the absence of SUN protein overexpression, while HIV-2 is largely unaffected. Stimulation of HIV-1 infection was also observed with bleomycin. Such a proviral effect of DNA damage has been previously observed in conditions of integrase inhibition (Ebina et al., 2012; Koyama et al., 2013). In contrast, it was previously reported that etoposide treatment inhibits HIV-1 infection in MDMs (Mlcochova et al., 2018). We speculate that this is explained by the presence of a SAMHD1-dependent block induced by etoposide in macrophages, but not in HeLa cells.

Similar to etoposide and bleomycin, ATR inhibition also enhances HIV-1 infection by 2-fold. The lack of a requirement for ATR in HIV infection is consistent with prior studies (Ariumi et al., 2005; Dehart et al., 2005). Interestingly, the effect of ATR inhibition requires the presence of the Vpr gene in HIV-1. As a virus-encoded gene, Vpr has been shown to induce an ATR-dependent G_2 arrest of the cell cycle (Zimmerman et al., 2006). Using purified and p24-normalized virus preparations, we made the unexpected observation that the Vpr-deficient virus is actually as infectious as the WT virus stimulated with ATR inhibition. In other words, in this asynchronous system of single-round infection of HeLa cells, the presence of the Vpr gene appears to provide a counter-intuitive 2-fold reduction in infectivity of the virus, which is alleviated by ATR inhibition. However, Vpr has been associated with an enhanced expression for the viral LTR during G_2 arrest (Goh et al., 1998). We speculate that in terms of viral replicative fitness, the reduction in single-round infectivity entailed by Vpr is cancelled out by this proviral effect of Vpr during G_2 arrest. Of note, both SUN1 and SUN2 overexpression inhibit HIV-1 infection irrespective of ATR inhibition. In contrast, etoposide rescues the antiviral effect of SUN2 on HIV-1, raising the possibility that ATR itself might play a role in the rescue of the SUN2 antiviral effect.

Multiple lines of evidence from our work indicate that the structure of the nuclear envelope impacts HIV infection. The ability of SR-KASH to partially rescue the antiviral effects of SUN proteins indicates that the LINC complex, which is located at the nuclear envelope, is involved. Despite the important morphological changes induced by SUN protein expression, we did not observe any change at the level of gene expression. This result suggests that SUN-mediated effects on the nucleus and HIV infection are post-transcriptional or that other changes in nucleic acid contents not assessed by our method are implicated. ATR is enriched at the nuclear envelope during the S phase and upon mechanical stretching, two processes that increase nuclear envelope stress (Kumar et al., 2014). ATR-deficient cells exhibit deformed nuclei, reminiscent of Lamin A/C depletion or SUN protein overexpression (Kidiyoor et al., 2020). Vpr overexpression was previously shown to induce herniations of the nuclear envelope associated with defects in the nuclear lamina (de Noronha et al., 2001). We also find that endogenous Lamin A/C has an antiviral effect, in agreement with a previous study (Sun et al., 2018).

We examined several effects of SUN protein overexpression and endogenous Lamin A/C on nuclear shape, deformability, NPC distribution and function, and chromatin dynamics. The effects on HIV-1 infection match the effects of the proteins on chromatin dynamics: decreased HIV-1 infection is associated with a decreased chromatin motility inside the nucleus and with decreased rotation of the nucleus relative to the cytoplasm. In contrast, HIV-2 infection is more susceptible to SUN2 than SUN1 and is not affected by Lamin A/C depletion. Overexpression of SUN2 deforms nuclei more than SUN1 but internal chromatin dynamics and nuclear rotation are less impacted. This strain specificity could be linked to a different dependency on host factors between HIV-1 and HIV-2 (Braaten and Luban, 2001). SUN and lamin proteins have been previously linked to chromatin mobility and nuclear rotation (Ji et al., 2007; Lottersberger et al., 2015; Oza et al., 2009; Ranade et al., 2019). Interestingly, nuclear rotation is required for optimal infection by another nuclear-invading virus, human cytomegalovirus (HCMV) (Procter et al., 2018). This rotation is required to promote spatial chromatin segregation that favors viral gene expression (Procter et al., 2018). We propose that HIV-1 infection requires nuclear rotation and chromatin movements for optimal integration and subsequent viral expression.

Our results highlight the interplay between HIV infection, structural proteins of the nuclear envelope, and the DNA damage response. Nuclear rotation and chromatin dynamics emerge as potentially important factors that control HIV infection. Future studies are required to address the underlying molecular mechanisms, which we anticipate will require the use of biophysical approaches. It will also be important to examine these mechanisms in the frame of the diversity of lentiviruses and their relevance for viral replication and innate immune sensing mechanisms in primary target cells.

STAR★METHODS

Detailed methods are provided in the online version of this paper and include the following:

- KEY RESOURCES TABLE
- RESOURCE AVAILABILITY
  - Lead contact
  - Materials availability
  - Data and code availability
- EXPERIMENTAL MODEL AND SUBJECT DETAILS
  - Cell lines and primary cultures
- METHOD DETAILS
  - Constructs
  - Virus production

- Cell transduction for protein overexpression or knockdown
- Cell infection
- DNA damage induction
- HIV DNA quantification
- Western blotting
- Live confocal imaging
- Confocal Immunofluorescence Imaging
- Fluorescence recovery after photobleaching
- Intracellular staining for flow cytometry
- Electron microscopy
- Micropipette aspiration microscopy
- Gene expression analysis by microarray

- QUANTIFICATION AND STATISTICAL ANALYSIS
- ADDITIONAL RESOURCES

SUPPLEMENTAL INFORMATION

Supplemental information can be found online at https://doi.org/10.1016/j.celrep.2021.109763.

ACKNOWLEDGMENTS

We thank V. Teixeira Rodrigues and J. Nikolic for assistance with primary macrophages; P. Benaroch for critically reading this manuscript; and M. Piel, N. De Silva, N. Jeremiah, V. Parissi, and F. Halary for discussions. We acknowledge the PICT-IBiSA imaging facility, member of the France-BioImaging national research infrastructure, supported by the CelTisPhyBio Labex (ANR-10-LBX-0038) part of the IDEX PSL (ANR-10-IDEX-0001-02 PSL), and Audrey Rapinat and David Gentien from the Genomics Platform at Institut Curie. This work was supported by Institut Curie, INSERM, and by grants from the Agence Nationale de la Recherche (ANR-10-IDEX-0001-02 PSL, ANR-11-LABX-0043, ANR-17-CE15-0025-01, ANR-19-CE15-0018-01, ANR-18-CE92-0022-01, and France-BioImaging ANR-10-INSB-04), the Agence Nationale de la Recherche sur le SIDA (ECTZ118797, ECTZ36691, ECTZ25472, and ECTZ71745), and Sidaction (VIH2016126002, 20-2-AEQ-12822-2, and 17-1-AAE-11097-2). A.B. was supported by fellowships from PSL University and Fondation pour la Recherche Médicale (grant no. 8250). P.M.D. was supported by fellowships from La Ligue contre le Cancer (REMX17751) and Fondation ARC (PDF20161205227).

AUTHOR CONTRIBUTIONS

A.B. performed experiments, analyzed data, and designed the study. A.W. contributed to some experiments. M.M. developed scripts for image analysis. P.M.D. performed the nuclear deformation assay. M.J. performed electron microscopy experiments. M.P. co-supervised A.W. X.L. assisted with the experimental setup and coordinated the study. N.M. designed and coordinated the study and wrote the first manuscript. All authors contributed to the text.

DECLARATION OF INTERESTS

The authors declare no competing interests.

Received: January 15, 2021
Revised: July 21, 2021
Accepted: September 3, 2021
Published: September 28, 2021

REFERENCES

Ariumi, Y., Turelli, P., Masutani, M., and Trono, D. (2005). DNA damage sensors ATM, ATR, DNA-PKcs, and PARP-1 are dispensable for human immunodeficiency virus type 1 integration. J. Virol. *79*, 2973–2978.

Bhargava, A., Lahaye, X., and Manel, N. (2018). Let me in: Control of HIV nuclear entry at the nuclear envelope. Cytokine Growth Factor Rev. *40*, 59–67.

Braaten, D., and Luban, J. (2001). Cyclophilin A regulates HIV-1 infectivity, as demonstrated by gene targeting in human T cells. EMBO J. *20*, 1300–1309.

Burke, B., and Stewart, C.L. (2013). The nuclear lamins: Flexibility in function. Nat. Rev. Mol. Cell Biol. *14*, 13–24.

Cerboni, S., Jeremiah, N., Gentili, M., Gehrmann, U., Conrad, C., Stolzenberg, M.C., Picard, C., Neven, B., Fischer, A., Amigorena, S., et al. (2017). Intrinsic antiproliferative activity of the innate sensor STING in T lymphocytes. J. Exp. Med. *214*, 1769–1785.

Davidson, P.M., Fedorchak, G.R., Mondésert-Deveraux, S., Bell, E.S., Isermann, P., Aubry, D., Allena, R., and Lammerding, J. (2019). High-throughput microfluidic micropipette aspiration device to probe time-scale dependent nuclear mechanics in intact cells. Lab Chip *19*, 3652–3663.

De Iaco, A., and Luban, J. (2014). Cyclophilin A promotes HIV-1 reverse transcription but its effect on transduction correlates best with its effect on nuclear entry of viral cDNA. Retrovirology *11*, 11.

de Noronha, C.M., Sherman, M.P., Lin, H.W., Cavrois, M.V., Moir, R.D., Goldman, R.D., and Greene, W.C. (2001). Dynamic disruptions in nuclear envelope architecture and integrity induced by HIV-1 Vpr. Science *294*, 1105–1108.

Dehart, J.L., Andersen, J.L., Zimmerman, E.S., Ardon, O., An, D.S., Blackett, J., Kim, B., and Planelles, V. (2005). The ataxia telangiectasia-mutated and Rad3-related protein is dispensable for retroviral integration. J. Virol. *79*, 1389–1396.

Dharan, A., Bachmann, N., Talley, S., Zwikelmaier, V., and Campbell, E.M. (2020). Nuclear pore blockade reveals that HIV-1 completes reverse transcription and uncoating in the nucleus. Nat. Microbiol. *5*, 1088–1095.

Donahue, D.A., Amraoui, S., di Nunzio, F., Kieffer, C., Porrot, F., Opp, S., Diaz-Griffero, F., Casartelli, N., and Schwartz, O. (2016). SUN2 overexpression deforms nuclear shape and inhibits HIV. J. Virol. *90*, 4199–4214.

Donahue, D.A., Porrot, F., Couespel, N., and Schwartz, O. (2017). SUN2 silencing impairs CD4 T cell proliferation and alters sensitivity to HIV-1 infection independently of cyclophilin A. J. Virol. *91*, e02303-16.

Ebina, H., Kanemura, Y., Suzuki, Y., Urata, K., Misawa, N., and Koyanagi, Y. (2012). Integrase-independent HIV-1 infection is augmented under conditions of DNA damage and produces a viral reservoir. Virology *427*, 44–50.

Foote, K.M., Nissink, J.W.M., McGuire, T., Turner, P., Guichard, S., Yates, J.W.T., Lau, A., Blades, K., Heathcote, D., Odedra, R., et al. (2018). Discovery and characterization of AZD6738, a potent inhibitor of ataxia telangiectasia mutated and Rad3 Related (ATR) kinase with application as an anticancer agent. J. Med. Chem. *61*, 9889–9907.

Goh, W.C., Rogel, M.E., Kinsey, C.M., Michael, S.F., Fultz, P.N., Nowak, M.A., Hahn, B.H., and Emerman, M. (1998). HIV-1 Vpr increases viral expression by manipulation of the cell cycle: A mechanism for selection of Vpr in vivo. Nat. Med. *4*, 65–71.

Gonzalo, S. (2014). DNA damage and lamins. In Cancer Biology and the Nuclear Envelope, E.C. Schirmer and J.I. de las Heras, eds. (Springer New York), pp. 377–399.

Ji, J.Y., Lee, R.T., Vergnes, L., Fong, L.G., Stewart, C.L., Reue, K., Young, S.G., Zhang, Q., Shanahan, C.M., and Lammerding, J. (2007). Cell nuclei spin in the absence of lamin B1. J. Biol. Chem. *282*, 20015–20026.

Kidiyoor, G.R., Li, Q., Bastianello, G., Bruhn, C., Giovannetti, I., Mohamood, A., Beznoussenko, G.V., Mironov, A., Raab, M., Piel, M., et al. (2020). ATR is essential for preservation of cell mechanics and nuclear integrity during interstitial migration. Nat. Commun. *11*, 4828.

Koyama, T., Sun, B., Tokunaga, K., Tatsumi, M., and Ishizaka, Y. (2013). DNA damage enhances integration of HIV-1 into macrophages by overcoming integrase inhibition. Retrovirology *10*, 21.

Kumar, A., Mazzanti, M., Mistrik, M., Kosar, M., Beznoussenko, G.V., Mironov, A.A., Garrè, M., Parazzoli, D., Shivashankar, G.V., Scita, G., et al. (2014). ATR mediates a checkpoint at the nuclear envelope in response to mechanical stress. Cell *158*, 633–646.

Lahaye, X., Satoh, T., Gentili, M., Cerboni, S., Conrad, C., Hurbain, I., El Marjou, A., Lacabaratz, C., Lelièvre, J.D., and Manel, N. (2013). The capsids of HIV-1 and HIV-2 determine immune detection of the viral cDNA by the innate sensor cGAS in dendritic cells. Immunity *39*, 1132–1142.

Lahaye, X., Satoh, T., Gentili, M., Cerboni, S., Silvin, A., Conrad, C., Ahmed-Belkacem, A., Rodriguez, E.C., Guichou, J.-F., Bosquet, N., et al. (2016). Nuclear envelope protein SUN2 promotes cyclophilin-A-dependent steps of HIV replication. Cell Rep. *15*, 879–892.

Lammerding, J., Schulze, P.C., Takahashi, T., Kozlov, S., Sullivan, T., Kamm, R.D., Stewart, C.L., and Lee, R.T. (2004). Lamin A/C deficiency causes defective nuclear mechanics and mechanotransduction. J. Clin. Invest. *113*, 370–378.

Lawrence, K.S., Tapley, E.C., Cruz, V.E., Li, Q., Aung, K., Hart, K.C., Schwartz, T.U., Starr, D.A., and Engebrecht, J. (2016). LINC complexes promote homologous recombination in part through inhibition of nonhomologous end joining. J. Cell Biol. *215*, 801–821.

Lei, K., Zhang, X., Ding, X., Guo, X., Chen, M., Zhu, B., Xu, T., Zhuang, Y., Xu, R., and Han, M. (2009). SUN1 and SUN2 play critical but partially redundant roles in anchoring nuclei in skeletal muscle cells in mice. Proc. Natl. Acad. Sci. USA *106*, 10207–10212.

Lei, K., Zhu, X., Xu, R., Shao, C., Xu, T., Zhuang, Y., and Han, M. (2012). Inner nuclear envelope proteins SUN1 and SUN2 play a prominent role in the DNA damage response. Curr. Biol. *22*, 1609–1615.

Liu, Q., Pante, N., Misteli, T., Elsagga, M., Crisp, M., Hodzic, D., Burke, B., and Roux, K.J. (2007). Functional association of Sun1 with nuclear pore complexes. J. Cell Biol. *178*, 785–798.

Lottersberger, F., Karssemeijer, R.A., Dimitrova, N., and de Lange, T. (2015). 53BP1 and the LINC complex promote microtubule-dependent DSB mobility and DNA repair. Cell *163*, 880–893.

Luo, X., Yang, W., and Gao, G. (2018). SUN1 regulates HIV-1 nuclear import in a manner dependent on the interaction between the viral capsid and cellular cyclophilin A. J. Virol. *92*, e00229-18.

Manel, N., Hogstad, B., Wang, Y., Levy, D.E., Unutmaz, D., and Littman, D.R. (2010). A cryptic sensor for HIV-1 activates antiviral innate immunity in dendritic cells. Nature *467*, 214–217.

Mangeot, P.E., Nègre, D., Dubois, B., Winter, A.J., Leissner, P., Mehtali, M., Kaiserlian, D., Cosset, F.L., and Darlix, J.L. (2000). Development of minimal lentivirus vectors derived from simian immunodeficiency virus (SIVmac251) and their use for gene transfer into human dendritic cells. J. Virol. *74*, 8307–8315.

Mlcochova, P., Caswell, S.J., Taylor, I.A., Towers, G.J., and Gupta, R.K. (2018). DNA damage induced by topoisomerase inhibitors activates SAMHD1 and blocks HIV-1 infection of macrophages. EMBO J. *37*, 50–62.

Oza, P., Jaspersen, S.L., Miele, A., Dekker, J., and Peterson, C.L. (2009). Mechanisms that regulate localization of a DNA double-strand break to the nuclear periphery. Genes Dev. *23*, 912–927.

Procter, D.J., Banerjee, A., Nukui, M., Kruse, K., Gaponenko, V., Murphy, E.A., Komarova, Y., and Walsh, D. (2018). The HCMV assembly compartment is a dynamic Golgi-derived MTOC that controls nuclear rotation and virus spread. Dev. Cell *45*, 83–100.e7.

Ranade, D., Pradhan, R., Jayakrishnan, M., Hegde, S., and Sengupta, K. (2019). Lamin A/C and Emerin depletion impacts chromatin organization and dynamics in the interphase nucleus. BMC Mol. Cell Biol. *20*, 11.

Rello-Varona, S., Gámez, A., Moreno, V., Stockert, J.C., Cristóbal, J., Pacheco, M., Cañete, M., Juarranz, A., and Villanueva, A. (2006). Metaphase arrest and cell death induced by etoposide on HeLa cells. Int. J. Biochem. Cell Biol. *38*, 2183–2195.

Roshal, M., Kim, B., Zhu, Y., Nghiem, P., and Planelles, V. (2003). Activation of the ATR-mediated DNA damage response by the HIV-1 viral protein R. J. Biol. Chem. *278*, 25879–25886.

Saini, M., and Potash, M.J. (2006). Novel activities of cyclophilin A and cyclosporin A during HIV-1 infection of primary lymphocytes and macrophages. J. Immunol. *177*, 443–449.

Schaller, T., Ocwieja, K.E., Rasaiyaah, J., Price, A.J., Brady, T.L., Roth, S.L., Hué, S., Fletcher, A.J., Lee, K., KewalRamani, V.N., et al. (2011). HIV-1 capsid-cyclophilin interactions determine nuclear import pathway, integration targeting and replication efficiency. PLoS Pathog. *7*, e1002439.

Schaller, T., Bulli, L., Pollpeter, D., Betancor, G., Kutzner, J., Apolonia, L., Herold, N., Burk, R., and Malim, M.H. (2017). Effects of inner nuclear membrane proteins SUN1/UNC-84A and SUN2/UNC-84B on the early steps of HIV-1 infection. J. Virol. *91*, e00463-17.

Schindelin, J., Arganda-Carreras, I., Frise, E., Kaynig, V., Longair, M., Pietzsch, T., Preibisch, S., Rueden, C., Saalfeld, S., Schmid, B., et al. (2012). Fiji: An open-source platform for biological-image analysis. Nat. Methods *9*, 676–682.

Schoggins, J.W., Wilson, S.J., Panis, M., Murphy, M.Y., Jones, C.T., Bieniasz, P., and Rice, C.M. (2011). A diverse range of gene products are effectors of the type I interferon antiviral response. Nature *472*, 481–485.

Silvin, A., Yu, C.I., Lahaye, X., Imperatore, F., Brault, J.B., Cardinaud, S., Becker, C., Kwan, W.H., Conrad, C., Maurin, M., et al. (2017). Constitutive resistance to viral infection in human $CD141^{+}$ dendritic cells. Sci. Immunol. *2*, eaai8071.

Singh, M., Hunt, C.R., Pandita, R.K., Kumar, R., Yang, C.-R., Horikoshi, N., Bachoo, R., Serag, S., Story, M.D., Shay, J.W., et al. (2013). Lamin A/C depletion enhances DNA damage-induced stalled replication fork arrest. Mol. Cell. Biol. *33*, 1210–1222.

Starr, T.K., Jameson, S.C., and Hogquist, K.A. (2003). Positive and negative selection of T cells. Annu. Rev. Immunol. *21*, 139–176.

Sun, W.-W., Jiao, S., Sun, L., Zhou, Z., Jin, X., and Wang, J.-H. (2018). SUN2 modulates HIV-1 infection and latency through association with lamin A/C to maintain the repressive chromatin. MBio. *9*, e02408–17.

Tseng, Q., Duchemin-Pelletier, E., Deshiere, A., Balland, M., Guillou, H., Filhol, O., and Théry, M. (2012). Spatial organization of the extracellular matrix regulates cell-cell junction positioning. Proc. Natl. Acad. Sci. USA *109*, 1506–1511.

Yamashita, M., and Engelman, A.N. (2017). Capsid-dependent host factors in HIV-1 infection. Trends Microbiol. *25*, 741–755.

Yamashita, M., Perez, O., Hope, T.J., and Emerman, M. (2007). Evidence for direct involvement of the capsid protein in HIV infection of nondividing cells. PLoS Pathog. *3*, 1502–1510.

Zhu, R., Antoku, S., and Gundersen, G.G. (2017). Centrifugal displacement of nuclei reveals multiple LINC complex mechanisms for homeostatic nuclear positioning. Curr. Biol. *27*, 3097–3110.e5.

Zimmerman, E.S., Sherman, M.P., Blackett, J.L., Neidleman, J.A., Kreis, C., Mundt, P., Williams, S.A., Warmerdam, M., Kahn, J., Hecht, F.M., et al. (2006). Human immunodeficiency virus type 1 Vpr induces DNA replication stress in vitro and in vivo. J. Virol. *80*, 10407–10418.

STAR★METHODS

KEY RESOURCES TABLE

REAGENT or RESOURCE	SOURCE	IDENTIFIER
Antibodies		
Actin (Clone C4)	Millipore	Cat# MAB1501, RRID: AB_2223041
Vinculin (Clone hVIN-1)	SIGMA	Cat# V9264, RRID: AB_10603627
SUN1 (EPR6554)	Abcam	Cat# ab124770 RRID:AB_10976056
SUN2	Atlas antibodies	Cat# HPA001209 RRID:AB_1080465
SUN2	Millipore	Cat# ABT272
Lamin A/C	Sigma	Cat# SAB4200236 RRID:AB_10743057
Lamin B2 clone LN43	Abcam	Cat #ab8983 RRID:AB_306912
NUP153	Sigma	Cat# HPA027896 RRID:AB_10611243
GFP Antibody Dylight 488 Conjugated Pre-Adsorbed (Polyclonal)	Rockland	Cat# 600-141-215 RRID: AB_1961516
HIV-1 p24 Clone KC57 – FITC	Beckman Coulter	Cat# 6604665 RRID:AB_1575987
H2AX p-S139 Clone N1-431	BD	Cat# 562377 RRID:AB_2737611
Mouse IgG1 κ isotype control Clone MOPC-21	BD	Cat# 554680 RRID:AB_395506
Rabbit-IgG (H+L) Alexa Fluor 546 conjugated	Invitrogen	Cat# A-11010 RRID:AB_2534077
Rabbit-IgG HRP-linked	Ozyme	Cat# 7074S RRID:AB_2099233
Mouse IgG HRP-linked	Ozyme	Cat# 7076S RRID:AB_330924
Bacterial and virus strains		
HIVGFP (NL4-3 strain)	Manel et al., 2010	Vif-, Vpr-, Vpu-, Env-, Nef-; GFP in Nef
HIVGFP N74D	Lahaye et al., 2016	Vif-, Vpr-, Vpu-, Env-, Nef-; GFP in Nef; CA mutation N74D
HIVGFP env-nef-	This study	Vif+, Vpr+, Vpu+, Env-, Nef-; GFP in Nef
HIVGFP env- nef- vpr-	This study	Vif+, Vpr-, Vpu+, Env-, Nef-; GFP in Nef
HIV-mTagBFP2 (NL4-3 strain)	This study	Vif-, Vpr-, Vpu-, Env-, Nef-; BFP in Nef
pLai ΔEnv GFP3	Yamashita et al., 2007	Vif+, Vpr+, Vpu+, Env-, Nef-; GFP
pTHRO.c/2626	NIH HIV Reagent Program ARP-11745	Full-length transmitter/founder HIV-1 clone
pCH058.c/2960	NIH HIV Reagent Program ARP-11856	Full-length transmitter/founder HIV-1 clone
pCH077.t/2627	NIH HIV Reagent Program ARP-11742	Full-length transmitter/founder HIV-1 clone
JR-CSF	Dan Littman lab, New York University	Full length HIV-1
YU-2	Dan Littman lab, New York University	Full length HIV-1
HIV-2 ROD9 ΔenvΔnef mTagBFP2+	This study	Vif+, Vpr+, Vpx+, Env-, Nef-; BFP in Nef
HIV-2 ROD9 ΔenvΔnef GFP	Manel et al., 2010	Vif+, Vpr+, Vpx+, Env-, Nef-; GFP in Nef
pJK7312As Δnef GFP+	Silvin et al., 2017	Vif+, Vpr+, Vpx+, Env+, Nef-; GFP in Nef
pSIV3+	Mangeot et al., 2000	/
Biological samples		
Human Healthy blood donors for primary PBMCs and MDMs	This manuscript	N/A
Human serum	Sigma	Cat# H4522
Chemicals, peptides, and recombinant proteins		
Human M-CSF	Miltenyi Biotec	Cat# 130-096-492
TransIT®-293 Transfection Reagent	Euromedex	Cat# MIR2706
Puromycin	Invivogen	Cat# ant-pr-1 CAS: 58-58-2
Protamine sulfate salt from salmon	SIGMA	Cat# P4020-1G CAS: 53597-25-4
Fetal bovine serum from Eurobio	Eurobio	Cat# CVFSVF0001

(*Continued on next page*)

Continued

REAGENT or RESOURCE	SOURCE	IDENTIFIER
Fetal bovine serum from GIBCO	Thermo Fisher Scientific	Cat# 10270-106
Fetal bovine serum from Corning	Thermo Fisher Scientific	Cat# 15377636
Penicillin-Streptomycin	Thermo Fisher Scientific	Cat# 15140122
Ficoll-Paque PLUS	Dutscher	Cat# 17-1440-03
Gentamicin (50mg/ml)	Thermo Fisher Scientific	Cat# 15750037
HEPES (1M)	Thermo Fisher Scientific	Cat# 15630080
DMEM, high glucose, GlutaMAX supplement	Thermo Fisher Scientific	Cat# 61965026
RPMI 1640 Medium, GlutaMAX supplement	Thermo Fisher Scientific	Cat# 61870010
cOmplete, EDTA-free, Protease inhibitor cocktails tablets	Roche	Cat# 11873580001
Azidothymidine	SIGMA	Cat# A2169; CAS: 30516-87-1; AZT
Nevirapine	SIGMA	Cat# SML0097; CAS: 129618-40-2; NVP
Cyclosporine A	Euromedex	Cat# S2286; CAS: 59865-13-3; CsA
Saponin from quillaja bark	Sigma Aldrich	S7900-100G
Goat serum	Sigma Aldrich	Cat# G9023-10ML
Fluoromount G with DAPI	eBioscience	Cat# 00-4959-52
Fluoromount G	eBioscience	Cat# 00-4958-02
SiR-DNA	Tebu-Bio	Cat# SC007
NucBlue DNA staining	Invitrogen	Cat# R37605
Etoposide	SIGMA	Cat# E1383-100MG CAS: 33419-42-0
Hydroxyurea	Sigma	Cat# H8627 CAS: 127-07-1
Bleomycin	Sigma	Cat# B8416 CAS: 9041-93-4
Q-VD-Oph	Selleckchem	Cat# S7311 CAS: 1135695-98-5
AZD6738	Selleckchem	Cat# S7693 CAS: 1352226-88-0
DMSO	VWR Chemicals	Cat# BDH1115 CAS: 67-68-5
Critical commercial assays		
Purelink HiPure Plasmid Midiprep Kit	Thermo Fisher Scientific	Cat# K210015
Nucleospin Gel and PCR Clean-Up kit	Macherey-Nagel	Cat# 740609.50
CD14 MicroBead human	Milteny Biotec	Cat# 130-050-201
LS columns	Milteny Biotec	Cat# 130-042-401
NucleoSpin RNA	Macherey-Nagel	Cat # 740955.50
NucleoSpin Tissue	Macherey-Nagel	Cat# 740952.50
LightCycler480 SYBR Green I Master	Roche	Cat# 4887352001
HIV-1 p24 ELISA Kit	Xpressbio	Cat# XB-1010
Foxp3 / Transcription Factor Staining Buffer Set	eBioscience	Cat# 00-5523-00
Deposited data		
Raw and analyzed data	This manuscript	NCBI GEO: GSE162019
Experimental models: Cell lines		
293FT	Thermo Fisher Scientific	Cat# R70007 RRID: CVCL_6911
HeLa	Laboratory of Dan Littman, New York University	N/A RRID: CVCL_0030
GHOST X4R5	NIH AIDS Reagent Program	Cat# 3942 RRID: CVCL_1E10
Oligonucleotides: See Table S1		
Recombinant DNA		
pCMV-VSVG	Manel et al., 2010	N/A
psPAX2	Manel et al., 2010	N/A
pTRIP-SFFV-tagBFP-2A	Cerboni et al., 2017	BFP
pTRIP-SFFV-TagRFP657-2A	This study	RFP657

(*Continued on next page*)

Continued

REAGENT or RESOURCE	SOURCE	IDENTIFIER
pTRIP-SFFV-EGFP	Lahaye et al., 2016	GFP
pTRIP-CMV-EGFP-2A		GFP
pTRIP-SFFV-tagBFP-2A-SUN1	This study (MGC cDNA cloneID: 40148817)	BFP
pTRIP-SFFV-tagBFP-2A-NtSUN2	This study	BFP
pTRIP-SFFV-tagBFP-2A-SUN1 Dharmacon (1-298)-ntSUN2 (220-717)	This study	BFP
pTRIP-SFFV-tagBFP-2A-NtSUN2 (1-219)-SUN1 Dharmacon (299-785)	This study	BFP
pTRIP-SFFV-TagRFP657-2A-SUN1 Dharmacon	This study (MGC cDNA cloneID: 40148817)	RFP657
pTRIP-SFFV-TagRFP657-2A-ntSUN2	This Study	RFP657
pTRIP-SFFV-EGFP-SR-KASH	This study	GFP
pLKO1puro-shLACZ	pLKO.1 clone ID TRCN0000072229	shRNA sequence: GCGATCGTAATCACCCGAGTG
pLKO.1-Puro-LMNA sh2	pLKO.1 clone ID TRCN0000061835	shRNA sequence: GAAGCAACTTCAGGATGAGAT
pLKO.1-Puro-LMNB2 sh5	pLKO.1 clone ID TRCN0000072422	shRNA sequence: CTACAAGTTCACGCCCAAGTA
Software and algorithms		
GraphPad Prism 7 and 8	GraphPad	https://www.graphpad.com/
Fiji	ImageJ	https://fiji.sc/
FlowJo	Tree Star	https://www.flowjo.com
Image Lab software – Version 5.2.1	BioRad	https://www.bio-rad.com/fr-fr/product/image-lab-software?ID=KRE6P5E8Z
LightCycler 480	Roche	https://lifescience.roche.com/en_fr/products/lightcycler14301-480-software-version-15.html
R	R Project	https://www.r-project.org
Bioconductor (packages listed in STAR methods)	Bioconductor	https://www.bioconductor.org

RESOURCE AVAILABILITY

Lead contact

Further information and requests for resources and reagents should be directed to and will be fulfilled by the lead contact, Nicolas Manel (nicolas.manel@curie.fr).

Materials availability

Plasmids generated in this study will be provided directly or through Addgene or similar service upon request.

Data and code availability

Gene expression data have been deposited at GEO and are publicly available as of the date of publication. The accession number is listed in the Key Resources Table. Microscopy data reported in this paper will be shared by lead contact upon request.

This paper does not report original code.

Any additional information required to reanalyze the data reported in this paper is available from the lead contact upon request.

EXPERIMENTAL MODEL AND SUBJECT DETAILS

Cell lines and primary cultures

GHOST (GHOST X4R5), 293FT and HeLa female cell lines were cultured in DMEM with Glutamax, 10% fetal bovine serum (FBS) (Corning), and penicillin-streptomycin (GIBCO). Human peripheral blood mononuclear cells (PBMCs) were isolated from buffy coats from normal human donors (approved by the Institut National de la Santé et de la Recherche Médicale ethics committee) using Ficoll-Paque PLUS (GE). $CD14^+$ cells were isolated by a positive selection with anti-human CD14 magnetic beads (Miltenyi) from PBMCs.

To obtain MDMs, $CD14^+$ cells were cultured in RPMI with Glutamax, 5% FBS (Eurobio), 5% human serum (Sigma), Penicillin-Streptomycin, Gentamicin (50 μg/ml, GIBCO) and HEPES (GIBCO) in the presence of recombinant human M-CSF (Miltenyi) at 50 ng/ml. Fresh media was added at day 5 or 6, and cells were treated/infected at day 9, after detachment via incubation with StemPro Accutase Cell Dissociation Reagent (GIBCO) for 30 minutes at 37°C. Drug treatments performed on cultured cells are listed in Key Resources Table.

METHOD DETAILS

Constructs

The plasmid constructs for lentiviral expression and HIV infection used in this study are listed in the Key Resources Table. pTRIP-SFFV-tagBFP-2A-SUN1 Dharmacon was generated by overlapping PCR cloning from commercially bought cDNA (MGC cDNA cloneID: 40148817) into pTRIP-SFFV-tagBFP-2A (Cerboni et al., 2017). pTRIP-SFFV-tagBFP-2A-ntSUN2 was generated by overlapping PCR mutagenesis from pLX304-SUN2 (Lahaye et al., 2016) into pTRIP-SFFV-tagBFP-2A with concomitant introduction of silent mutations that are not targeted by SUN2 shRNA 4 and 5 (respectively GAGCCTATTCAGACGTTTCACTTT to GAACCGATCCAAAC TTTCCATTTC and AAGAGGAAATCCAGCAACATGAAG to AAACGCAAGAGTTCTAATATGAAA). pTRIP-SFFV-tagBFP-2A-SUN1 Dharmacon (1-298)-ntSUN2 (220-717) and pTRIP-SFFV-tagBFP-2A-ntSUN2 (1-219)-SUN1 Dharmacon (299-785) were generated by overlapping PCR cloning from the full-length constructs. pTRIP-SFFV-tagRFP657-2A-SUN1 and pTRIP-SFFV-tagRFP657-2A-ntSUN2 were generated via restriction enzyme digestion from the tagBFP expressing vectors and ligation into pTRIP-SFFV-TagRFP657-2A backbone. HIV-GFP env-nef- was generated by PCR-mediated insertion of the Vpr+Vif+Vpu+ cassette from NL4-3 into HIV-GFP (Manel et al., 2010). HIV-GFP env-nef-vpr- was generated by overlapping PCR mutagenesis from HIV-GFP env-nef-, introducing a frameshift mutation within *vpr,* after the codon corresponding to amino-acid I63 (gaattc to gaaTTAAttc). HIV-mTagBFP2 and HIV-2 ROD9 ΔenvΔnef mTagBFP2+ were obtained via overlapping PCR mutagenesis, replacing GFP with the mTagBFP from pTRIP-SFFV-mTagBFP-2A.

Virus production

Viral particles were produced by transfection of 293FT cells in 6-well plates with 3 μg DNA and 8 μL TransIT-293 Transfection Reagent (Mirus Bio) per well. For VSV-G pseudotyped SIVmac virus-like particles (VLPs), 0.4 μg CMV-VSVG and 2.6 μg $pSIV3^+$ was used. For VSV-G pseudotyped HIV-1 and HIV-2 viruses used in the study, 0.4 μg CMV-VSVG and 2.6 μg HIV DNA was used. For overexpression or shRNA mediated knock-down, 0.4 μg CMV-VSVG, 1 μg psPAX2 and 1.6 μg of lentivector of interest were combined. One day after transfection, media was removed, cells were washed once, and 3 mL per well of RPMI medium with Glutamax, 10% FBS (GIBCO), PenStrep (GIBCO), 50 μg/ml Gentamicin (GIBCO) and 0.01 M HEPES (GIBCO) were added. Viral supernatants were harvested 1 day later, filtered using 0.45 μm pore filters, used fresh or aliquoted and frozen at −80°C. When required, the virus was purified and concentrated on a 20% sucrose cushion in phosphate buffered saline (PBS) in Ultra Clear Centrifuge tubes (Beckman Coulter), via ultracentrifugation at 4°C at 31,000 *x g* in a SW32Ti swinging bucket rotor (Beckman Coulter). Viral pellets were then resuspended in complete medium at a 100-fold concentration compared to crude. Viral titers were measured on GHOST cells (titration as previously described (Manel et al., 2010) or using HIV-1 p24 ELISA (XpressBio). ELISA absorbance acquisitions were acquired on a FLUOstar OPTIMA (BMG Labtech) and data were analyzed and exported to Excel with MARS Data Analysis Software (BMG Labtech).

Cell transduction for protein overexpression or knockdown

HeLa cells were counted and seeded in 6-well plates on the day prior to transduction. Purified virus was added at a 2:1 volume ratio on medium containing protamine at a final concentration of 1 μg/ml. $CD14^+$ monocytes were seeded in 10-cm dishes in the presence of 50 ng/ml M-CSF to induce differentiation into macrophages and transduced with purified SIVmac VLPs and lentiviruses carrying vector of interest, mixed at a 1:1 ratio. Human serum was added at day 1 post transduction. Transductions of monocytes was performed in the presence of protamine at a final concentration of 1 μg/ml. HeLa cells were washed once in PBS and passaged at 48 hours post transduction with or without 2 μg/ml of puromycin. For MDMs, medium was replaced at day 5-6 post transduction. Overexpression was assessed by quantification of fluorescent reporter signal via flow cytometry on a BD FACSVerse flow cytometer. Both overexpression and protein knock-down were confirmed by Western Blotting at day of experiment.

Cell infection

HeLa, GHOST and MDMs (day 8-9 post transduction) were seeded and infected in the presence of 1 μg/ml of protamine with serial dilutions of frozen viral stocks in a BSL-3 laboratory. For HIV-1 and HIV-2, viruses made with the plasmids HIVGFP (NL4-3 strain) and HIV-2 ROD9 ΔenvΔnef GFP (ROD strain), respectively, were used in most experiments, except noted otherwise. Virus was removed at 48 hours post-infection, cells were washed, harvested, stained for viability using Fixable Viability Dye eFluor 780 in PBS where required, fixed in 1% paraformaldehyde (PFA; Electron Microscopy Sciences) and analyzed for GFP, BFP or p24 positivity via flow cytometry on a BD FACSVerse flow cytometer. Viral titers were calculated based on seeded cell number and the percentages of infected cells, within the linear range of infection.

DNA damage induction

For chemical induction of DNA damage, HeLa cells were seeded in 12-well plates 24 hours prior to treatment and infection. The following day, cell medium was replaced with complete medium containing 1 μg/ml of protamine and different concentrations of either etoposide, hydroxyurea or bleomycin (Sigma). Corresponding concentrations of diluents DMSO or water were used as non-treated controls. Cells were infected immediately after treatment, as described above. Four hours later, drugs and viruses were removed and cells were washed once with PBS. 1mL of fresh medium per well was added and cells were put back in culture for 44 hours. In the case of etoposide treatment, medium was supplemented with 50 mM of Q-VD-Oph to allow cell survival. One control well per treatment condition was harvested at either 4 or 24 hours post treatment, for intranuclear γH2AX staining, as described.

For UV irradiation, HeLa cells were seeded in 12-well plates 24 hours prior to irradiation and infection. Media was replaced the following day to include 1 μg/ml of protamine and cells were UV irradiated at a 1 mJ/cm^2 setting for 2 s using UVILink *CL 508 Crosslinkers* from *UVITec*. Infection was performed immediately after irradiation and cells were left in culture for another 48 hours. One control well per irradiation condition was harvested at 4 hours post irradiation, for intranuclear γH2AX staining, as described.

HIV DNA quantification

HeLa cells and MDMs were infected as described, with the addition of infected wells treated with reverse transcriptase inhibitors as negative control. For this purpose, either 24 μM of AZT (Sigma) or 10 μM of NVP (Sigma) were used. After 24 hours, cells were washed in PBS and harvested. Total DNA was extracted from cell pellets using NucleoSpin Tissue (Macherey-Nagel) kit, as per manufacturer's protocol. Quantitative real-time PCR analysis was performed in a Roche LightCycler 480 with Roche 480 SYBR Green I master reagent in 20 mL final volume per well according to manufacturer specifications as previously described (Lahaye et al., 2013). Each sample was measured in triplicate for all primers. For beta-globin, primers were bglobin-f and bglobin-r. Cycling conditions were 1x 95°C for 5′; 35x 95°C for 10'', 65°C for 20'' (50°C for beta-globin) and 72°C for 30''. Relative concentrations of total DNA (Late RT), 2-LTR circles and integrated viral DNA were calculated relative to beta-globin using the ΔCt method. The primers used are listed in Table S1.

Western blotting

0.5 to 1 million cells were lysed in 100 μL of RIPA buffer (50 mM Tris HCl, 150 mM NaCl, 0.1% SDS, 0.5% DOC, 1% NP-40, Protease inhibitor (Roche; 1187358001)). Lysis was performed on ice for 30'. Lysates were cleared by centrifugation at 8000 g for 8 minutes at 4°C, 20 μl of Laemmli 6x (12% SDS, 30% Glycerol, 0.375 M Tris-HCl pH 6.8, 30% 2-mercaptoethanol, 1% bromophenol blue) was added and samples were boiled at 95°C for 15'. Cellular protein lysates were resolved on Criterion or 4% – 20% Bio-Rad precast SDS-PAGE gels and transferred to PVDF membranes (Bio-Rad). Membranes were saturated and proteins were blotted with antibodies in 5% non-fat dry milk, PBS 0.1% Tween buffer. ECL signal generated via Clarity Western ECL substrate (Bio-Rad) was recorded on the ChemiDoc-XRS or ChemiDoc Touch Bio-Rad Imager. Data were analyzed and quantified with the Image Lab software (Bio-Rad). The antibodies used in this study are listed in the Key Resources Table.

Live confocal imaging

For live imaging, HeLa cells were plated either in a glass bottom FluoroDish (World Precision Instruments) or in a glass-bottom Cellview Cell Culture Dish with 4 compartments (Greiner Bio-One), on the day prior to experiments. One hour before imaging, cells were incubated with either 1 μM of SiR-DNA (Tebu Bio) or 2 drops of NucBlue Live Ready Probes (Invitrogen), directly in the culture medium, at 37°C. Images of cells were acquired with a Leica DmI8 inverted microscope equipped with an SP8 confocal unit using a 20x dry objective (NA = 0.75, pixel size was fixed to 0.284 μm). Imaging was performed in an on-stage incubator chamber at 37°C, with 5% CO_2. An image per condition was taken every 2 or 6 minutes, depending on the experiment.

Image analysis was performed using Fiji software (Schindelin et al., 2012). For chromatin dynamics analysis, a homemade macro was first used to do segmentation of each nucleus on the Video and identify them using the 3D object counter. Particle Image Velocimetry (PIV) analysis was then performed on SiR-DNA staining using the PIV plug-in (Tseng et al., 2012). PIV is a basic optic flow analysis, that divides each image of a stack in small clusters of pixels (interrogation windows) and measures the displacement of each cluster between pairs of consecutive frames. The cross-correlation then generates a pattern of ''movements'' within the nucleus that are color-coded based on the amplitude of the vector corresponding to the displacement of each cluster. An in-house script was used to first align each individual nucleus, then measure and average SiR-DNA displacements over the ten first time points. Red shades indicate higher amplitudes of displacement while violets correspond to quasi-immobile clusters. For nuclear rotation analysis, a macro was used to measure rotation angles across the first 30 frames. Briefly, individual nuclei were first aligned using a translation transformation of the MultiStackReg plug-in (Brad Busse, Stanford), then they were aligned using the rotation transformation and the transformation was applied to a reference image containing 2 fixed points (one at the center and one on the edge) to measure the rotation. A threshold of 1 degree/minute was used to define rotating nuclei. The percentage of rotation time and the average velocity was then computed.

Confocal Immunofluorescence Imaging

For immunofluorescence, HeLa cells were grown overnight onto 12 mm glass coverslips (Thermo Scientific) placed in 6-well plates. For nuclear shape quantification, 1 μM of SiR-DNA was added in cell culture media and cells were incubated for 2 hours at 37°C. Cells

were then fixed with 4% PFA for 20 minutes at room temperature. Coverslips were washed multiple times with PBS and quenched with 0.1 M Glycine in PBS (Life Technologies) for 10 minutes at room temperature. For nuclear shape quantification, coverslips were washed multiple times in PBS, rinsed once in distilled water and were ready for mounting and imaging. For intracellular staining, coverslips were further blocked with PBS, 0.2% (w/v) bovine serum albumin (BSA) (Euromedex), 0.05% (w/v) Saponin from quillaja bark (SIGMA) for 30 minutes at room temperature. Cells were stained overnight with anti-NUP153 antibody at 2 μg/mL (1:50 dilution) or with Normal Rabbit IgG Isotype Control at corresponding concentration of the primary antibody, in PBS, 0.2% (w/v) BSA, 0.05% (w/v) Saponin + 10% goat serum (Sigma), at 4°C in a humidified chamber. The following day, cells were washed multiple times and incubated with the secondary antibody Alexa Fluor 546 goat anti-rabbit IgG (H+L) (Invitrogen; 1:200 dilution in PBS-BSA-Saponin) in the presence of 1 μM of SiR-DNA for 2 hours in the dark, at room temperature. Coverslips were washed multiple times in PBS-BSA-Saponin and finally rinsed once in distilled water. Coverslips for all experiments were mounted onto glass slides using Fluoromount G (eBioscience) mounting medium. The slides were finally dried at 37°C for 1h and stored at 4°C. Cells were imaged with a Leica DmI8 inverted microscope equipped with an SP8 confocal unit using an oil immersion 63x objective (NA = 1.4) for NUP-153 staining or an oil immersion 40x objective (N = 1.3) for nuclear shape measurement, with applied Type F Immersion Liquid (Leica).

Fluorescence recovery after photobleaching

Cells were seeded at 2.5 × 10^5 cells/dish in a glass bottom FuoroDish (World Precision Instruments) on the day prior to the experiment. Cells were imaged with a Leica DmI8 inverted microscope equipped with an SP8 confocal unit using a 20x dry objective (NA = 0.75). Imaging was performed in an on-stage incubator chamber at 37°C, with 5% CO_2. Two independent modules were used in a sequential manner: one for bleaching, one for imaging the signal recovery. During the application of the bleaching module, the 488 laser was focused at an intensity of 5% and with a gain of 0.1% on to an area within the nucleus of each cell at maximum zoom for 20 s. Immediately afterward, the first sequence was manually cancelled, the resolution was optimized, imaging area was restored to the whole cell for the second sequence. The laser power was set for optimal imaging level and images of the whole cell were acquired for 3 min circa at the rate of one image every 2.2 s.

Intracellular staining for flow cytometry

Cell surface staining was performed in PBS, 1% BSA (Euromedex), 1 mM EDTA (GIBCO), 0.01% NaN3 (AMRESCO) (FACS Buffer) at 4°C. Viability staining (Live-Dead) with Fixable Viability Dye eFluor 780 was performed in PBS at 4°C. Intracellular p24 staining was carried out as follows: 48 hours after infection, cells were extensively washed with PBS, harvested and fixed/stained using the BD Cytoperm/Cytofix kit, as per manufacturer's protocol, using the anti-HIV-1 core antibody clone KC57 coupled to FITC. Intracellular staining of γH2AX was performed using the FOXP3/Transcription Factor Staining Buffer Set (eBioscience) as per manufacturer's protocol. Cells were resuspended in FACS Buffer prior to final acquisition. All flow cytometry acquisitions were performed on the FACSVerse (BD) using the FACSSuite software (BD) and analyzed on FlowJo v10. The antibodies used are listed in the Key Resources Table.

Electron microscopy

Cells were seeded at 5 × 10^4 cells/well in a 24w plate onto sterile 12 mm glass coverslips (Thermo Scientific) and left to adhere overnight. The following morning, cells were washed in PBS and were fixed using 2% glutaraldehyde in 0.1 M cacodylate buffer, pH 7.4 for 1h, post fixed for 1h with 2% buffered osmium tetroxide, dehydrated in a graded series of ethanol solution, and then embedded in epoxy resin. Images were acquired with a digital 4k CCD camera Quemesa (EMSIS GmbH, Münster, Germany) mounted on a Tecnai Spirit transmission electron microscope (ThermoFisher, Eindhoven, the Netherlands) operated at 80kV.

Micropipette aspiration microscopy

Prior to harvest, HeLa cell lines were incubated with 1 μM SiR-DNA dye from Tebu Bio for 1h30 at 37°C in cell culture medium. Cells were washed, harvested, and resuspended at a concentration of 5x10^6 cells/mL in sterile 3% BSA in PBS-0.2% FBS. Cells were subjected to the experimental conditions as described previously (Davidson et al., 2019).

Gene expression analysis by microarray

We performed three independent experiments with control, SUN1 and SUN2 expressing cells. Total RNA was extracted from 10^6 HeLa cells using NucleoSpin RNA and adjusted to 50 ng/μL. A WT PLUS amplification and labeling protocol was conducted with 100 ng of total RNA. Samples passed the quality control with a high score. The Affymetrix analysis was performed by the NGS platform at Institut Curie using the Human Gene 2.0 ST chip. Human Gene 2.0ST array were scanned using a Genechip 7G scanner, according to the supplier's protocol. Micro-array analyses were processed with R using packages from Bioconductor. The quality control was performed using ArrayQualityMetrics package without detecting any outlier among the experiment. Data were normalized using the Robust Multi-Array Average algorithm from the Oligo package. Annotation of the probes was done using the hugene20 annotation data (chip hugene20sttranscriptcluster) from Bioconductor. Differential gene-expression analysis was performed with Limma.

QUANTIFICATION AND STATISTICAL ANALYSIS

Statistical analyses were performed in Prism 7 or 8 (GraphPad Software). The statistical tests used, as well as statistical parameters including the exact value of n, dispersion, and precision measures, are reported in the figures and figure legends. In the figures, significance is indicated as follows: *p < 0.05, **p < 0.01, ***p < 0.001; ****p < 0.0001; ns, not statistically significant.

ADDITIONAL RESOURCES

The graphical abstract was created with BioRender.com.